Received 29 November 2022; accepted 26 December 2022. Date of publication 2 January 2023; date of current version 11 January 2023.

Digital Object Identifier 10.1109/OJCOMS.2022.3233423

Map-Assisted Constellation Design for mmWave WDM With OAM in Short-Range LOS Environment

YUAN WANG[1,2], CHEN GONG[1,2] (Senior Member, IEEE), NUO HUANG[1,2], AND ZHENGYUAN XU[1,2] (Senior Member, IEEE)

[1]Key Laboratory of Wireless-Optical Communications, Chinese Academy of Sciences, Beijing 100045, China

[2]School of Information Science and Technology, University of Science and Technology of China, Hefei 230026, China

CORRESPONDING AUTHORS: C. GONG and N. HUANG (e-mail: cgong821@ustc.edu.cn; huangnuo@ustc.edu.cn)

This work was supported in part by the National Natural Science Foundation of China under Grant 62171428 and Grant 62101526; in part by the Key Program of National Natural Science Foundation of China under Grant 61631018; in part by the Key Research Program of Frontier Sciences of CAS under Grant QYZDY-SSW-JSC003; and in part by the Fundamental Research Funds for the Central Universities under Grant KY2100000118.

ABSTRACT We consider a system that integrates positioning and single-user millimeter wave (mmWave) communication, where the communication part adopts wavelength division multiplexing (WDM) and orbital angular momentum (OAM). This paper addresses the multi-dimensional constellation design in short-range line-of-sight (LOS) environment, with stable communication links. We propose a map-assisted method to quantify the system parameters based on positions and reduce real-time computing overhead. We explore the possibility of using a few patterns in the maps, and investigate its performance loss. We first investigate the features of OAM beams, and find that the link gain ratio between any two sub-channels remains unchanged at some specific positions. Then, we prove that a fixed constellation can be adopted for the positions where the link gain matrices are sufficiently close to be proportional. Moreover, we prove that the system can adopt a fixed power vector to generate a multi-dimensional constellation if the difference between fixed power vector and optimal power vector is small. Finally, we figure out that the constellation design for all receiver positions can be represented by a few constellation sets.

INDEX TERMS Millimeter wave communication, multi-dimensional constellation, orbital angular momentum, wavelength division multiplexing, short-range line-of-sight.

I. INTRODUCTIONS

CURRENTLY, intelligent terminals are becoming more and more widely deployed, which provide not only positioning, tracking and other sensing services, but also high-speed communication services [1]. However, with the development of communication technologies, the demand for spectrum resource is increasing. Such trend calls for high-frequency spectrum like millimeter wave (mmWave) and terahertz (THz) [2], [3]. In this work, we mainly consider mmWave spectrum. Compared with sub-6GHz communication, mmWave communication can occupy wider spectrum resource (30-300 GHz) to guarantee high-speed transmission [4]. On the other hand, orbital angular momentum (OAM), as a new degree of freedom, is applied to mmWave systems to further increase the transmission rate [5], [6], [7], [8].

Due to the characteristics of beam diffusion and coaxial transmission, OAM is only suitable for short-range line-of-sight (LOS) communication [7], [9], [10], [11]. Moreover, higher spectrum will lead to larger propagation, penetration and reflection losses [12], [13], which further limits the application to short-range LOS environment. In most existing mmWave systems, data processing is performed only in a single continuous spectrum, even with wide bandwidth [14], [15], and the advantage of mmWave with abundant continuous or separate spectrum can be further utilized [16], [17]. Benefiting from the large link losses, mmWave systems can aggregate the licensed or unlicensed broad spectrum with small external interference to increase transmission rate. In general, broad spectrum communication is combined with wavelength division multiplexing (WDM) technology,

which adopts multiple carrier wavelengths to transmit data streams [18], [19].

For mmWave spectrum communication in sparsely scattered environment, such as conference room and workshop, the influence of multi-path is limited and the LOS path is dominant [20]. Meanwhile, the mmWave propagation shows an apparent quasi-optical property according to experimental measurement [21]. Hence, the mmWave short-range LOS link can be considered as a pure LOS channel [12]. Based on the above feature, the link conditions of mmWave communication in short-range LOS environment are only related to the positions of transmitter and receiver [22]. Generally, high accuracy positioning is necessary for some short-range intelligent systems, such as industrial Internet and indoor robot. If OAM is adopted, this position information can be used to align the receiving antenna axis with transmitting antenna axis. Certainly, the systems can directly utilize OAM signals to locate and communicate [22], [23].

Motivated by the quasi-static feature and positioning-communication integration, we attempt to configure the communication system based on the transceiver's position. Due to the stable gains for short-range LOS links, the optimal system parameters are determined when the position information is obtained. Hence, we construct a look-up table, which is termed as map method, to store the system parameters of all interested positions [24]. Adopting map-assisted approach has two potential advantages: (1) For the system whose positioning service is active, the transmitter and receiver always have position information. If a communication request appears, the system can directly configure the transmitter and receiver by adopting the parameters stored in the map. Since there is no need for the time and transmission symbol overhead of channel estimation, channel feedback and real-time optimization, the delay of initial communication establishment will be reduced. (2) The system can solve computationally intensive optimization problems in an offline manner and store the optimization results into the map, which significantly relaxes the real-time computational pressure.

The major contributions of this paper can be summarized as follows:

- We consider a mmWave WDM system with different OAM modes in a short-range LOS scenario. To improve the system detection performance, we mainly focus on the multi-dimensional constellation design problem, which generally can be converted to the maximization of the minimum Euclidean distance (MED) between any two constellation symbols.
- With the quasi-static nature of mmWave channel in short-range LOS environment, we construct a multi-dimensional constellation map to store the optimal constellation sets for different receiver positions. To reduce the map size, we adopt clustering method to classify all positions of interest into several categories, and use the same constellation at all positions of each category. We adopt the normalized MED difference as the performance criterion for clustering.
- To analyze the feature of multi-dimensional constellation at different receiver positions, we first investigate the characteristics of OAM beams with different wavelengths and modes, and figure out that the link gain matrices can be proportional at certain positions. Then, we prove that a fixed constellation can be adopted for the positions where the link gain matrices are sufficiently close to be proportional. Besides, we also consider the system with fixed power allocation and prove that the system can adopt a fixed power vector to generate a multi-dimensional constellation if the difference between the fixed power vector and optimal power vector is small. The claim of the above theoretical analysis is supported by the numerical results.

The remainder of this paper is organized as follows. In Section II, we provide the system model, elaborate the features of OAM beams and display the configuration process of map-assisted systems. In Section III, we investigate the multi-dimensional constellation design, analyze the features of link gain ratio, figure out that the same link gain ratio leads to the same constellation, and that the constellation design can be represented by only a few constellation sets in the map. Moreover, we also investigate the effect of fixed power allocation on constellation design. Section IV presents some numerical results to verify our theoretical analysis. Finally, Section V concludes this paper.

II. SYSTEM MODEL

Consider a short-range LOS mmWave system, which is equipped with a positioning module, as shown in Figure 1. To aggregate the licensed or unlicensed broad spectrum, we adopt the WDM technique. In addition, we adopt the OAM technique to further increase the data rate.

For WDM, we consider the system with I carrier wavelengths. As shown in Figure 1, there are $I = 3$ carrier wavelengths, namely λ_1, λ_2 and λ_3. The transmitter and receiver of each carrier wavelength both equip an OAM antenna, and the interval between the centers of any two adjacent antennas is d_a. Assume that the receiver of each carrier wavelength equips a perfect band-pass filter to remove the inter-carrier interference. Since the antenna of each carrier wavelength can multiplex several OAM modes, the whole system can be considered to be composed of I parallel mmWave OAM sub-systems.

For OAM, we utilize traveling-wave antennas or spiral phase plates (SPPs) at the transmitter side to generate Laguerre-Gaussian (LG) beams with different OAM modes under the coaxial condition [5], [6], [7], [8], [25]. At the receiver side, we adopt a uniform circular array (UCA) [26], [27], as shown in the Rx part of Figure 1, to reduce the detection complexity.

The localization can be performed by additional positioning techniques, e.g., ultra-wideband and visible light

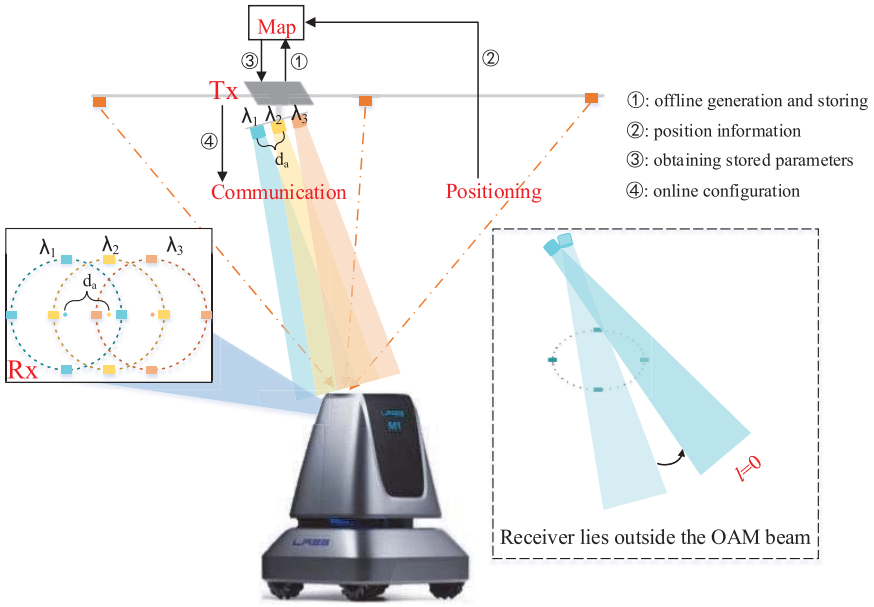

FIGURE 1. The scenario of the intelligent terminal equipped with mmWave WDM and OAM system.

positioning [28], or directly utilizing the communication links [22], [23]. Since we only focus on the communication part in this work, we assume the position information is available to the terminal and can be fed back to the transmitter. Benefiting from the position information, the transmitting and receiving antennas are generally considered to be aligned [7], [11], which can also be realized by tracking schemes [29], [30]. According to the characteristics of the LG beam, the receiver may lie outside the beam, as shown in the lower right part of Figure 1. In this case, the system can transmit only plane wave (i.e., the OAM mode number is $l = 0$), ignoring the alignment condition. However, in this paper, we mainly investigate the features of OAM beam region, and does not consider the system design for the region outside OAM beam.

We adopt LG method to characterize OAM beams [5], [31]. In cylindrical coordinate, the channel response on the i-th carrier with OAM mode l at position (r, ϕ, z) is given by [5], [31]

$$h_i^l(r,\phi,z) = \frac{\sqrt{\zeta_i^l}\lambda_i}{4\pi d_{i,m}^l(z)}\left(\frac{r}{r_{i,max}^l(z)}\right)^{|l|} e^{\frac{\left(\left(r_{i,max}^l(z)\right)^2 - r^2\right)}{\omega_i^2(z)}} \cdot e^{-j\frac{\pi\left(r^2-\left(r_{i,max}^l(z)\right)^2\right)}{\lambda_i R_i^l(z)}} e^{-j\frac{2\pi}{\lambda_i}d_{i,m}^l(z)} e^{-jl\phi}, \tag{1}$$

where ϕ is the transverse azimuthal angle [32]; λ_i is the carrier wavelength; $\omega_i(z) = \omega_i\sqrt{1+(\frac{z}{z_R})^2}$ is the beam spot of the fundamental Gaussian beam and ω_i is the beam waist radius; $z_R = \frac{\pi\omega_i^2}{\lambda_i}$ is the Rayleigh distance and assumed the same for all sub-systems; $R_i^l(z) = z\left[1+\left(\frac{\pi\omega_i^2}{\lambda_i z}\right)^2\right]$ is the curvature radius; $r_{i,max}^l(z) = \sqrt{\frac{|l|}{2}}\omega_i(z) = \omega_i\sqrt{\frac{|l|}{2}\left(1+\left(\frac{z}{z_R}\right)^2\right)}$ is the radius of maximum energy strength region, in which the channel response follows Frris law [5], [33]; $d_{i,m}^l(z) = \sqrt{(r_{i,max}^l(z))^2 + z^2}$; $e^{-jl\phi}$ denotes the helical phase distribution of OAM wave with mode l; ζ_i^l incorporates both antenna gain and system loss of i-th sub-system with OAM mode l and is assumed to be 1. Therefore, the link gain can be written as

$$\begin{aligned} g_i^l(r,z) &= \left|h_i^l(r,z)\right|^2 \\ &= \frac{\lambda_i^2}{(4\pi)^2\left(d_{i,m}^l(z)\right)^2}\left(\frac{r}{r_{i,max}^l(z)}\right)^{2|l|} e^{\frac{2\left(\left(r_{i,max}^l(z)\right)^2 - r^2\right)}{\omega_i^2(z)}}. \end{aligned} \tag{2}$$

According to Equation (1), the channel response can be represented as $h_i^l(r,\phi,z) = h_i^l(r,z)e^{-jl\phi}$. Due to inter-mode orthogonality, the OAM-based systems can coaxially transmit multiple OAM beams without inter-channel interference (ICI). We assume the same OAM modes employed in each sub-system, which can be perfectly separated at the receiver.

Figure 1 also presents the process of the map-assisted method. The system solves optimization problems at all positions in an offline manner, classifies these results into a few patterns, and then stores these results into a map. After obtaining the position information, the system looks up the parameters from the map and configures the transmitter and receiver by adopting these parameters. Note that, if the system lies in an environment with lots of small-scale fading, the channel gain cannot be determined even if the position of the transceiver is fixed. Therefore, the obtained map is not applicable in this scenario. In this paper, we mainly consider the mmWave frequency and short-range LOS environment, where the links are sparse and quasi-static. Apparently, quantization error will mismatch the position together with its

optimal parameters, leading to performance loss. In the following section, we theoretically analyze the performance loss in the multi-dimensional constellation design and find the features in maps via combination with numerical results.

III. MULTI-DIMENSIONAL CONSTELLATION MAP FOR MMWAVE WDM SYSTEMS

In this section, we consider multi-dimensional constellation design and analyze the performance loss when adopting map-assisted approach.

A. MULTI-DIMENSIONAL CONSTELLATION DESIGN

We assume that all OAM parallel sub-channels jointly carry one multi-dimensional symbol. Let $\mathcal{L}$ denote the set of OAM modes, $L = |\mathcal{L}|$ denote the number of OAM modes in any sub-system, and $U = IL$ denote the total number of sub-channels. The sub-channel set is denoted by $\{1, 2, \ldots, U\}$. The multi-dimensional constellation set is denoted by $\mathcal{C} \triangleq \{\mathbf{x}_1, \mathbf{x}_2, \ldots, \mathbf{x}_M\}$ with $\mathbf{x}_m \in \mathbb{C}^U$. We assume that the bandwidth of each sub-channel is the same.

At the receiver, the received signal can be written as $\mathbf{y} = \mathbf{H}\mathbf{x}_m + \mathbf{n}$ if codeword $\mathbf{x}_m$ is sent, where $\mathbf{H} \in \mathbb{C}^{U\times U}$ is the parallel channel matrix assumed to be diagonal due to axis alignment and perfect band-pass filter in each sub-channel; $\mathbf{n} \in \mathbb{C}^U$ is the additive Gaussian noise vector with zeros mean and covariance matrix $N_0\mathbf{I}$. The mean error probability of symbol detection under channel matrix $\mathbf{H}$ can be written as

$$\bar{P}_e = \frac{1}{M}\sum_{m=1}^{M}\sum_{n\neq m}\int_{D_n} P(\mathbf{y}|\mathbf{x}_m, \mathbf{H})d\mathbf{y}, \tag{3}$$

where D_n is the decision region of symbol $\mathbf{x}_n$. Generally, it is difficult to obtain the closed-form expression of $\bar{P}_e$, and we can adopt the following upper bound instead,

$$\bar{P}_e \leq (M-1)Q\left(\sqrt{\frac{d^2_{min}(\mathbf{H}, \mathcal{C})}{2N_0}}\right), \tag{4}$$

where $d_{min}(\mathbf{H}, \mathcal{C}) \triangleq \min_{\mathbf{x}_m, \mathbf{x}_n\in\mathcal{C}, m\neq n} \|\mathbf{H}(\mathbf{x}_m - \mathbf{x}_n)\|_2$ is the MED; $Q(\cdot)$ is the tail probability of the standard normal distribution. From Equation (4), it is seen that the minimization of $\bar{P}_e$ can be converted to the maximization of $d_{min}(\mathbf{H}, \mathcal{C})$, regardless of the noise power N_0. Hence, we maximize the MED for multi-dimensional constellation design [34].

Denoting $D \triangleq 2U$, we stack all symbol vectors of $\mathcal{C}$ to a single $MD \times 1$ column vector as

$$\mathbf{x_p} = \left[\mathrm{Re}\{\mathbf{x}_1\}^T, \mathrm{Im}\{\mathbf{x}_1\}^T, \ldots, \mathrm{Re}\{\mathbf{x}_M\}^T, \mathrm{Im}\{\mathbf{x}_M\}^T\right]^T, \tag{5}$$

where $\mathrm{Re}\{\cdot\}$ and $\mathrm{Im}\{\cdot\}$ represent the element-wise operations of extracting the real and imaginary components of a vector, respectively; $\{\cdot\}^T$ represents the transpose operation. The Euclidean distance of two symbols $\mathbf{x}_m$ and $\mathbf{x}_n$ can be rewritten as $\mathbf{x_p}^T\mathbf{E}_{mn}\mathbf{x_p}$, where

$$\mathbf{E}_{mn} = \begin{bmatrix} \ddots & & & & \\ & \mathbf{V_D} & & -\mathbf{V_D} & \\ & & \ddots & & \\ & -\mathbf{V_D} & & \mathbf{V_D} & \\ & & & & \ddots \end{bmatrix}_{MD\times MD}, \tag{6}$$

$\mathbf{V_D} \in \mathcal{R}^{D\times D}$ is given by

$$\mathbf{V}_D = \begin{bmatrix} \mathbf{H}^H\mathbf{H} & \mathbf{0} \\ \mathbf{0} & \mathbf{H}^H\mathbf{H} \end{bmatrix}, \tag{7}$$

$(\cdot)^H$ represents the conjugate transpose operation. In $\mathbf{E}_{mn}$, the (m, m)-th and (n, n)-th $D\times D$ blocks are $\mathbf{V_D}$; the (m, n)-th and (n, m)-th blocks are $-\mathbf{V_D}$; and other elements are all zero. The constellation optimization problem can be formulated as

$$\begin{aligned} \max_{\mathbf{x_p}} \ & d_{min} \\ \text{s.t.} \ & \mathbf{x_p}^T\mathbf{E}_{mn}\mathbf{x_p} \geq d^2_{min}, \quad \forall m, n, 1 \leq m < n \leq M, \\ & \frac{1}{M}\left\|\mathbf{x_p}\right\|_2^2 \leq P_{sum}, \end{aligned} \tag{8}$$

where P_{sum} denotes the total transmit power and is set as $P_{sum} = 1$ in this paper. The constraint $\mathbf{x_p}^T\mathbf{E}_{mn}\mathbf{x_p} \geq d^2_{min}$ is non-convex and can be approximately transformed into the following linear constraint:

$$\begin{aligned} \mathbf{x_p}^T\mathbf{E}_{mn}\mathbf{x_p} &\approx 2\cdot\mathbf{x_p}^T_{(k-1)}\mathbf{E}_{mn}\mathbf{x_{p}}_{(k)} - \mathbf{x_p}^T_{(k-1)}\mathbf{E}_{mn}\mathbf{x_{p}}_{(k-1)} \\ &\geq d^2_{min}, \quad \forall m, n, 1 \leq m < n \leq M. \end{aligned} \tag{9}$$

Based on Equation (9), the optimization problem (8) can be solved via an iterative procedure (subscript k represents the k-th iteration), which is generally computationally intensive due to the high optimization dimension, especially when U or M is large. For example, when $I = 2$, $L = 2$ and $M = 64$, the optimization dimension of $\mathbf{x_p}$ is $2M \times L \times I = 512$, resulting in the difficulty of real-time optimization. A multi-dimensional constellation map can be constructed as a look-up table to reduce the real-time computational complexity.

B. MULTI-DIMENSIONAL CONSTELLATION MAP

We characterize the constellation design according to the receiver location. We quantize all receiver locations of interest into various sampling regions, and calculate the optimal multi-dimensional constellation at the center position of each sampling region. We assume that the above optimal multi-dimensional constellation set can well represent the constellation sets at all positions of this sampling region, especially when the sampling interval is sufficiently small.

In general, the receiver moves in a three-dimensional (3D) space. Since the link gain is independent of azimuth angle ϕ, the 3D map can be reduced due to rotational symmetry, and we can only consider vertical distance z along the axis and horizontal distance r from the axis. As shown in

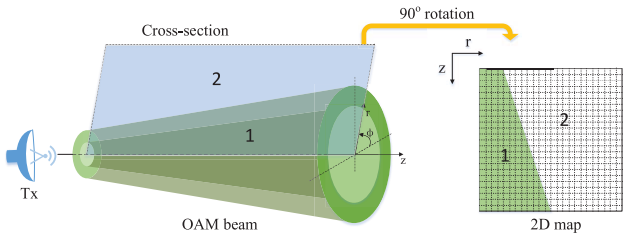

FIGURE 2. The OAM transmission in the 3D space, and the arbitrary cross-section.

Figure 2, the two-dimensional (2D) map is an arbitrary cross-section of the OAM beam. The 2D map is divided into two regions, where region 1 is covered by the OAM beam and region 2 lies outside the OAM beam. The multi-Dimensional Constellation map can be generated according to the 2D map and provide prior knowledge to configure the transceiver.

To reduce the storing and searching demand of look-up table, some effective methods (e.g., clustering, interpolation, and parallelization) can be adopted [24], [35]. In this work, a clustering method is adopted to classify all positions of interest into several categories. It is expected that for all positions in a category, the system can adopt the same constellation set, which is the optimal constellation set for a certain position in this category. Such constellation set can be generated in an offline manner, and stored in a look-up table. We adopt normalized MED difference as the criterion of the clustering process. Hence, the above situation is similar to that, for any two positions q_1 and q_2, if the normalized MED difference at position q_2 using the constellation set for position q_1 is sufficiently small, the system at these two positions can adopt the same constellation set (i.e., the constellation set for position q_1). The normalized MED difference can be expressed as

$$\Delta\bar{d}_{min}(q_1, q_2) = \left| 1 - \frac{d_{min}\left(\mathbf{H}^{(q_2)}, \mathcal{C}^{(q_1)}\right)}{d_{min}\left(\mathbf{H}^{(q_2)}, \mathcal{C}^{(q_2)}\right)} \right|, \tag{10}$$

where $\mathbf{H}^{(q_2)}$ is the channel matrix at position q_2; $\mathcal{C}^{(q_1)}$ and $\mathcal{C}^{(q_2)}$ are the optimal multi-dimensional constellations for positions q_1 and q_2, respectively.

The clustering approach is summarized in Algorithm 1, which is specified as follows. We randomly select a position q_a from the position set $\mathcal{Q}$ with the optimal multi-dimensional constellation $\mathcal{C}^{(q_a)}$. For other positions $\{q_t\}$, if the normalized MED differences $\{\Delta\bar{d}_{min}(q_a, q_t)\}$ are lower than a certain preset threshold $\tau_{d_{min}}$, we classify these positions and q_a into one category, and remove these positions from $\mathcal{Q}$. Moreover, the constellation of this category is set to be $\mathcal{C}^{(q_a)}$. The random position selection and classification continue until all positions are classified into certain categories. Then, we calculate the total normalized MED difference $\Delta\bar{d}_s$, which is the summation of the normalized MED differences at all positions. We repeat the whole above process C_d times and select the results with the lowest $\Delta\bar{d}_s$ to generate the multi-dimensional constellation map $\mathcal{C}_{map}$. In this paper, we set $\tau_{d_{min}} = 0.15$ and $C_d = 100$.

Algorithm 1 Constellation Clustering Algorithm

Input: Position set $\mathcal{Q} \triangleq \{q_1, q_2, \ldots, q_{|\mathcal{Q}|}\}$, multi-dimensional constellation sets at all positions $\mathfrak{C} \triangleq \{\mathcal{C}^{(1)}, \mathcal{C}^{(2)}, \ldots, \mathcal{C}^{(|\mathcal{Q}|)}\}$, distortion threshold $\tau_{d_{min}}$, repetition times C_d.

for $d = 1 : C_d$ **do**
  Let $t = 0$, $T = 0$, the number of categories $\kappa^{[d]} = 0$, the total normalized MED difference be $\Delta\bar{d}_s^{[d]}$, $\mathcal{Q}^{[d]} = \mathcal{Q}$.
  while $|\mathcal{Q}^{[d]}|! = 0$ **do**
    Randomly select a position q_a from $\mathcal{Q}^{[d]}$.
    $T = |\mathcal{Q}^{[d]}|$, $\kappa^{[d]} = \kappa^{[d]} + 1$, $\mathbf{N}_{\kappa^{[d]}} = \{q_a\}$.
    for $t = 1 : T$ **do**
      Let q_t be the t-th element of $\mathcal{Q}^{[d]}$.
      if $q_t == q_a$ **then**
        continue;
      end if
      if $\Delta\bar{d}_{min}(q_a, q_t) < \tau_{d_{min}}$ **then**
        $\mathbf{N}_{\kappa^{[d]}} = \{\mathbf{N}_{\kappa^{[d]}}, q_t\}$, $\mathcal{Q}^{[d]} = \mathcal{Q}^{[d]} \setminus q_t$.
        $\Delta\bar{d}_s^{[d]} = \Delta\bar{d}_s^{[d]} + \Delta\bar{d}_{min}(q_a, q_t)$.
      end if
    end for
  end while
  Record $\Delta\bar{d}_s^{[d]}$, $\kappa^{[d]}$, $\mathbf{N}_1, \mathbf{N}_2, \ldots, \mathbf{N}_{\kappa^{[d]}}$.
end for
Select the records with the lowest $\Delta\bar{d}_s^{[d^*]}$ as the final results, where $d^* = \arg\min_{d=1,\ldots,C_d} \Delta\bar{d}_s^{[d]}$.

Output: The number of categories $\kappa^{[d^*]}$, the position sets of different categories $\mathbf{N}_1, \mathbf{N}_2, \ldots, \mathbf{N}_{\kappa^{[d^*]}}$, the map $\mathcal{C}_{map} \triangleq \{\mathcal{C}^{(\mathbf{N}_1\{1\})}, \mathcal{C}^{(\mathbf{N}_2\{1\})}, \ldots, \mathcal{C}^{(\mathbf{N}_{\kappa^{[d^*]}}\{1\})}\}$.

TABLE 1. Descriptions of parameters.

Parameters	Descriptions
$(\cdot)^{(1)}$	Superscript (1) represents position 1
$(\cdot)^{l}$	Superscript l represents the l-th OAM mode
$(\cdot)_i$	Subscript i represents the i-th carrier wavelength
β	Horizontal distance from the beam axis
λ_a	An arbitrary carrier wavelength
l_m	An arbitrary nonzero OAM mode
$a_{i,j}^{l}$	Link gain ratio between the i-th and j-th wavelengths
$a_i^{l_1,l_2}$	Link gain ratio between mode l_1 and mode l_2
$\mathbf{x}_{\mathcal{C}^{(1)}}^{(1)}, \tilde{\mathbf{x}}_{\mathcal{C}^{(1)}}^{(1)}$	MED constellation pair for $\alpha\mathbf{H}^{(1)}$ using $\mathcal{C}^{(1)}$
$\beta_{i,max}^{l}$	The horizontal distance with the maximum link gain
$\mathcal{S}^{(o)}$, $\mathcal{S}^{(f)}$	The optimal constellation sets under $\mathbf{p}^{(o)}$ and $\mathbf{p}^{(f)}$
$\mathbf{s}_f^{(o)}, \tilde{\mathbf{s}}_f^{(o)}$	MED constellation pair for $\mathbf{p}^{(o)}$ using $\mathcal{S}^{(f)}$

C. MED-DIFFERENCE ANALYSIS ON MULTI-DIMENSIONAL CONSTELLATION MAP

In this subsection, we theoretically analyze the conditions under which the system can adopt the same multi-dimensional constellation set. We mainly focus on the normalized MED difference, which can further determine the feature of the multi-dimensional constellation map. Since there are plenty of parameters in this part, we list the descriptions of these parameters in Table 1, where we only list one example if multiple parameters have similar definitions.

1) VARIATION OF LINK GAINS AT DIFFERENT RECEIVER POSITIONS

Since the multi-dimensional constellation mainly depends on the channel condition of each sub-channel, we first investigate the channel characteristics for different receiver positions. To facilitate the analysis, we consider link gain $g_i^l(r,z)$ rather than channel response $h_i^l(r,\phi,z)$, and focus on the link gain ratios within OAM beam regions, where $\mathcal{L}$ consists of several OAM modes. Denote λ_a as an arbitrary carrier wavelength. Let $r=\beta r_{a,max}^{l_m}(z)$, where β is a non-negative number and l_m is an arbitrary nonzero OAM mode. It is seen that when λ_a and l_m are fixed, radius r can be replaced by β to determine the horizontal distance from the beam axis. Consider two sub-channels with different wavelengths λ_i and λ_j, $1\le i,j\le I$, and the same OAM mode $l\in\mathcal{L}$. Denoting $a_{i,j}^l(\beta,z)\triangleq\frac{g_i^l(\beta r_{a,max}^{l_m}(z),z)}{g_j^l(\beta r_{a,max}^{l_m}(z),z)}$ for $\lambda_i>\lambda_j$, we have

$$a_{i,j}^l(\beta,z)=\left(\frac{\lambda_j}{\lambda_i}\right)^{|l|-2}\frac{\omega_j^2\frac{|l|}{2}\left(1+\frac{z^2}{z_R^2}\right)+z^2}{\omega_i^2\frac{|l|}{2}\left(1+\frac{z^2}{z_R^2}\right)+z^2}e^{\beta^2|l_m|\left(\frac{\lambda_i}{\lambda_j}-1\right)}. \tag{11}$$

Note that term $\frac{\omega_j^2\frac{|l|}{2}\left(1+\frac{z^2}{z_R^2}\right)+z^2}{\omega_i^2\frac{|l|}{2}\left(1+\frac{z^2}{z_R^2}\right)+z^2}$ increases monotonically with z and converges to 1 when $\lambda_i>\lambda_j$. Moreover, this term converges rapidly because $\omega^2=z_R\lambda/\pi\ll 1$ in short-range mmWave systems. For instance, considering that $l=+2$, $z_R=4$ m and two carrier frequencies $f_i=60$ GHz and $f_j=65$ GHz, this term is larger than 0.995 for $z>0.1$ m. Hence, the above link gain ratio can be approximated as $a_{i,j}^l(\beta,z)\approx\left(\frac{\lambda_j}{\lambda_i}\right)^{|l|-2}e^{\beta^2|l_m|\left(\frac{\lambda_i}{\lambda_j}-1\right)}$. Then, consider two sub-channels with different OAM modes $l_1,l_2\in\mathcal{L}$, and the same wavelength λ_i, $1\le i\le I$. Assume $|l_1|$ and $|l_2|$ are small integers (e.g., $l_1=+2$ and $l_2=+1$). Denoting $a_i^{l_1,l_2}(\beta,z)\triangleq\frac{g_i^{l_1}(\beta r_{a,max}^{l_m}(z),z)}{g_i^{l_2}(\beta r_{a,max}^{l_m}(z),z)}$ for $|l_1|>|l_2|$, we have

$$a_i^{l_1,l_2}(\beta,z)\approx\left(\frac{\lambda_a}{\lambda_i}\right)^{|l_1|-|l_2|}\left(\beta^2|l_m|\right)^{|l_1|-|l_2|}\frac{|l_2|^{|l_2|}}{|l_1|^{|l_1|}}e^{|l_1|-|l_2|}. \tag{12}$$

Considering the following link gain ratios at two different positions (β_1,z_1) and (β_2,z_2), we have

$$\begin{aligned}\frac{a_{i,j}^{l,(1)}}{a_{i,j}^{l,(2)}}&=\frac{a_{i,j}^l(\beta_1,z_1)}{a_{i,j}^l(\beta_2,z_2)}=e^{|l_m|\left(\frac{\lambda_i}{\lambda_j}-1\right)(\beta_1^2-\beta_2^2)},\\ \frac{a_i^{l_1,l_2,(1)}}{a_i^{l_1,l_2,(2)}}&=\frac{a_i^{l_1,l_2}(\beta_1,z_1)}{a_i^{l_1,l_2}(\beta_2,z_2)}=\left(\frac{\beta_1}{\beta_2}\right)^{2(|l_1|-|l_2|)}.\end{aligned} \tag{13}$$

According to Equation (13), the link gain ratios are primarily determined by β_1 and β_2, and are both equal to 1 if $\beta_1=\beta_2$. This indicates that for the positions with the same β, $a_{i,j}^l$ and $a_i^{l_1,l_2}$ remain unchanged, i.e., all sub-channels have uniform link gain ratio. More specifically, for any i,j $(1\le i,j\le I)$ and l_1,l_2 $(l_1,l_2\in\mathcal{L})$, the link gains of two sub-channels satisfy $g_i^{l_1}=a_{i,j}^{l_1}g_j^{l_1}=a_{i,j}^{l_1}a_j^{l_1,l_2}g_j^{l_2}$. For any two positions 1 and 2 with the same β, since $a_{i,j}^{l_1}$ and $a_j^{l_1,l_2}$ remain unchanged, we have $g_i^{l_1,(1)}=a_{i,j}^{l_1}a_j^{l_1,l_2}g_j^{l_2,(1)}$ and $g_i^{l_1,(2)}=a_{i,j}^{l_1}a_j^{l_1,l_2}g_j^{l_2,(2)}$. Letting $g_j^{l_2,(2)}=\alpha^2g_j^{l_2,(1)}$, where α is a positive number, we have $g_i^{l_1,(2)}=\alpha^2g_i^{l_1,(1)}$. Hence, denoting link gain matrix $\mathbf{G}\triangleq\mathrm{diag}(g_1^{l_1},\ldots,g_1^{l_L},\ldots,g_I^{l_1},\ldots,g_I^{l_L})$ with $\mathrm{diag}(\cdot)$ being the diagonalization operation, we have $\mathbf{G}^{(2)}=\alpha^2\mathbf{G}^{(1)}$. The above analysis shows that the link gains of different sub-channels vary proportionally at different positions with the same β. We call that these positions satisfy the uniform link gain ratio.

2) THE IMPACT OF CHANNEL CONDITION ON MULTI-DIMENSIONAL CONSTELLATION DESIGN

Then, we explore the influence of channel condition on the multi-dimensional constellation design. Since channel matrix $\mathbf{H}$ is diagonal, we have $\mathbf{G}=\mathbf{H}^H\mathbf{H}$. For any two positions with the same β, we have $\mathbf{G}^{(2)}=\alpha^2\mathbf{G}^{(1)}$, which can further lead to ${\mathbf{H}^{(2)}}^H\mathbf{H}^{(2)}=\alpha^2{\mathbf{H}^{(1)}}^H\mathbf{H}^{(1)}$. Combining Equations (6) and (7), the first constraint under $\mathbf{H}^{(2)}$ can be expressed as

$$\begin{aligned}{\mathbf{x}_\mathbf{p}}^T\mathbf{E}_{mn}^{(2)}\mathbf{x}_\mathbf{p}=\alpha^2\cdot{\mathbf{x}_\mathbf{p}}^T\mathbf{E}_{mn}^{(1)}\mathbf{x}_\mathbf{p}\ge d_{min}^2,\\ \forall m,n,1\le m<n\le M.\end{aligned} \tag{14}$$

It is easy to see that the original optimization problem (8) under $\mathbf{H}^{(2)}$ is equivalent to that under $\mathbf{H}^{(1)}$, with only scaling difference.

For OAM beam region, the variations of the link gains in different sub-channels are proportional only at the positions with the same β, and are not proportional at other positions. Hence, we consider the influence of this non-proportional channel variation. Considering two positions with the channel matrices $\mathbf{H}^{(1)}$ and $\mathbf{H}^{(2)}$, we always have $\mathbf{H}^{(2)}=\alpha\mathbf{H}^{(1)}+\Delta\mathbf{H}$, where $\Delta\mathbf{H}$ stands for the deviation. Different α will lead to different $\Delta\mathbf{H}$. Note that ${\mathbf{H}^{(2)}}^H\mathbf{H}^{(2)}=(\alpha\mathbf{H}^{(1)}+\Delta\mathbf{H})^H(\alpha\mathbf{H}^{(1)}+\Delta\mathbf{H})$. Let $\mathcal{C}^{(1)}$ and $\mathcal{C}^{(2)}$ denote the optimal multi-dimensional constellation sets for $\alpha\mathbf{H}^{(1)}$ and $\mathbf{H}^{(2)}$, respectively. Assume that $\{\mathbf{x}_{\mathcal{C}^{(1)}}^{(1)},\tilde{\mathbf{x}}_{\mathcal{C}^{(1)}}^{(1)}\}$ and $\{\mathbf{x}_{\mathcal{C}^{(2)}}^{(1)},\tilde{\mathbf{x}}_{\mathcal{C}^{(2)}}^{(1)}\}$ are the corresponding MED constellation pairs for $\alpha\mathbf{H}^{(1)}$ using $\mathcal{C}^{(1)}$ and $\mathcal{C}^{(2)}$, respectively; $\{\mathbf{x}_{\mathcal{C}^{(1)}}^{(2)},\tilde{\mathbf{x}}_{\mathcal{C}^{(1)}}^{(2)}\}$ and $\{\mathbf{x}_{\mathcal{C}^{(2)}}^{(2)},\tilde{\mathbf{x}}_{\mathcal{C}^{(2)}}^{(2)}\}$ are the corresponding MED constellation pairs for $\mathbf{H}^{(2)}$ using $\mathcal{C}^{(1)}$ and $\mathcal{C}^{(2)}$, respectively. Then, we have the following result on the normalized MED difference.

Theorem 1: Given diagonal matrices $\mathbf{H}^{(1)}$ and $\mathbf{H}^{(2)}$ that satisfy $\mathbf{H}^{(2)}=\alpha\mathbf{H}^{(1)}+\Delta\mathbf{H}$, we have the following upper bound

$$\begin{aligned}\Delta\bar{d}_{min}^{\Delta\mathbf{H}}&\triangleq 1-\frac{d_{min}\left(\mathbf{H}^{(2)},\mathcal{C}^{(1)}\right)}{d_{min}\left(\mathbf{H}^{(2)},\mathcal{C}^{(2)}\right)}\\ &\le\frac{\|\Delta\mathbf{H}\|_F\left(\|\mathbf{x}_{\mathcal{C}^{(2)}}^{(1)}-\tilde{\mathbf{x}}_{\mathcal{C}^{(2)}}^{(1)}\|_2+\|\mathbf{x}_{\mathcal{C}^{(1)}}^{(2)}-\tilde{\mathbf{x}}_{\mathcal{C}^{(1)}}^{(2)}\|_2\right)}{\|\mathbf{H}^{(2)}\left(\mathbf{x}_{\mathcal{C}^{(2)}}^{(2)}-\tilde{\mathbf{x}}_{\mathcal{C}^{(2)}}^{(2)}\right)\|_2}.\end{aligned} \tag{15}$$

Generally, term $(\|\mathbf{x}^{(1)}_{\mathcal{C}^{(2)}} - \tilde{\mathbf{x}}^{(1)}_{\mathcal{C}^{(2)}}\|_2 + \|\mathbf{x}^{(2)}_{\mathcal{C}^{(1)}} - \tilde{\mathbf{x}}^{(2)}_{\mathcal{C}^{(1)}}\|_2)/\|\mathbf{H}^{(2)}(\mathbf{x}^{(2)}_{\mathcal{C}^{(2)}} - \tilde{\mathbf{x}}^{(2)}_{\mathcal{C}^{(2)}})\|_2$ is finite, and we have $\Delta\bar{d}^{\Delta\mathbf{H}}_{min} = O(\|\Delta\mathbf{H}\|_F)$.

Proof: See Appendix A. ∎

Since $d_{min}(\mathbf{H}^{(2)}, \mathcal{C}^{(2)}) \geq d_{min}(\mathbf{H}^{(2)}, \mathcal{C}^{(1)})$ always holds, we have $\Delta\bar{d}^{\Delta\mathbf{H}}_{min} \geq 0$. Theorem 1 indicates that the order of the asymptotic convergence rate of $\Delta\bar{d}^{\Delta\mathbf{H}}_{min}$ with respect to $\Delta\mathbf{H}$ is not larger than that of $\|\Delta\mathbf{H}\|_F$. Hence, $\Delta\bar{d}^{\Delta\mathbf{H}}_{min}$ can be sufficiently small if $\|\Delta\mathbf{H}\|_F$ is sufficiently small, and the systems under $\mathbf{H}^{(1)}$ and $\mathbf{H}^{(2)}$ can adopt the same multi-dimensional constellation set. As link gain is continuous and monotonous with respect to channel response, the sufficiently small $\|\Delta\mathbf{H}\|_F$ can lead to a sufficiently small difference between $\mathbf{G}^{(2)}$ and $\alpha^2\mathbf{G}^{(1)}$, namely $\mathbf{G}^{(1)}$ and $\mathbf{G}^{(2)}$ are sufficiently close to be proportional.

Since it is difficult to obtain an accurate theoretical position variation range, we attempt to qualitatively analyze the classification. According to the definition of $r^l_{i,max}(z)$, it is easy to obtain $r^l_{i,max}(z) = \sqrt{\frac{\lambda_i|l|}{\lambda_a|l_m|}}r^{l_m}_{a,max}(z)$. Since $r = \beta r^{l_m}_{a,max}(z)$, we define $\beta^l_{i,max} \triangleq \sqrt{\frac{\lambda_i|l|}{\lambda_a|l_m|}}$ to represent the horizontal distance with the maximum link gain for any z. For any $l \neq 0$, assuming $0 < \Delta\beta < \beta^l_{i,max}$, we have

$$a_r \triangleq \frac{g^l_i\left(\beta^l_{i,max} + \Delta\beta, z\right)}{g^l_i\left(\beta^l_{i,max} - \Delta\beta, z\right)} = \left(1 + \frac{2\Delta\beta}{\beta^l_{i,max} - \Delta\beta}\right)^{2|l|} e^{\frac{|l_m|\lambda_a}{\lambda_i}4\Delta\beta\beta^l_{i,max}}. \quad (16)$$

Since $\partial a_r/\partial\Delta\beta > 0$ always holds, we have $a_r > a_r|_{\Delta\beta=0} = 1$. This implies that the signal strength in the left region of $\beta^l_{i,max}$ decays more rapidly than that in the right region as $\Delta\beta$ increases. More specifically, compared with range $\beta > \beta^l_{i,max}$, the channel matrix $\mathbf{H}$ changes more rapidly within range $0 < \beta < \beta^l_{i,max}$ and thus $\|\Delta\mathbf{H}\|_F$ is larger when given a same $\Delta\beta$. Hence, there will be multiple categories in the left region of $\beta^l_{i,max} = \sqrt{\frac{\lambda_i|l|}{\lambda_a|l_m|}}$ in the multi-dimensional constellation map. Compared with the right region of $\beta^l_{i,max}$, the areas of these categories will be smaller.

3) THE IMPACT OF POWER ALLOCATION ON MULTI-DIMENSIONAL CONSTELLATION DESIGN

Then, we also consider the power pre-allocation system, where the power in each sub-channel is configured only when the communication link is established, but not convenient for real-time adjustment. This situation will occur when the system adopts multiple separate transmitters, such as SPPs, to generate different OAM beams [6]. Once the communication link is established, the system can be considered as adopting fixed power allocation. Letting $\mathbf{p} \triangleq [P_1, P_2, \ldots, P_U]^T$ denote the allocated power vector over all sub-channels and $\mathbf{A} \triangleq \sqrt{\text{diag}(\mathbf{p})}$, the multi-dimensional constellation symbol $\mathbf{x} \in \mathcal{C}$ satisfying $\mathbf{x} = \mathbf{A}\mathbf{s}$, where $\mathbf{s}$ is the multi-dimensional constellation symbol removing power matrix $\mathbf{A}$. Let $\mathcal{S} \triangleq \{\mathbf{s}_1, \mathbf{s}_2, \ldots, \mathbf{s}_M\}$ denote the set of $\mathbf{s}$. The MED can be rewritten as $d_{min}(\mathbf{H}, \mathbf{p}, \mathcal{S}) = \|\mathbf{H}\mathbf{A}(\mathbf{s}_m - \mathbf{s}_n)\|_2$, where $\mathbf{s}_m$ and $\mathbf{s}_n$ are the MED constellation pair of $\mathcal{S}$. Moreover, each sub-channel has individual power constraint, and the second constraint of the optimization problem (8) can be replaced by $\frac{1}{M}\|\mathbf{J}_n\mathbf{x}_\mathbf{p}\|^2_2 \leq P_n, \forall n \in \{1, 2, \ldots, U\}$, where $\mathbf{J}_n = \text{diag}(\mathbf{J}(n, :))$ and $\mathbf{J}$ is the $MD \times MD$ sub-channel selection matrix with only 0 and 1 elements. Since the first constraint remains unchanged, Theorem 1 still holds in this case.

Compared with the system with total power constraint system, since the power in each sub-channel is difficult to change, the system with fixed power vector may suffer a large performance loss. However, we can confirm that this performance loss can be small at some positions where the difference between the fixed power vector and the optimal power vector is small. Assume that $\mathbf{p}^{(o)}$ and $\mathbf{p}^{(f)}$ are the optimal and fixed power allocation vectors, respectively. $\mathbf{p}^{(o)}$ can be extracted from the optimal multi-dimensional constellation set $\mathcal{C}^{(o)}$. Assume $\mathcal{S}^{(o)}$ and $\mathcal{S}^{(f)}$ are the optimal constellation sets for $\mathbf{H}$ under $\mathbf{p}^{(o)}$ and $\mathbf{p}^{(f)}$, respectively. In this part, the subscripts $(\cdot)_o$ and $(\cdot)_f$ indicate that the constellation symbols belong to the sets $\mathcal{S}^{(o)}$ and $\mathcal{S}^{(f)}$, respectively. At any position with the channel matrix $\mathbf{H}$, assume that $\{\mathbf{s}^{(o)}_o, \tilde{\mathbf{s}}^{(o)}_o\}$ and $\{\mathbf{s}^{(o)}_f, \tilde{\mathbf{s}}^{(o)}_f\}$ are the corresponding MED constellation pairs for $\mathbf{p}^{(o)}$ using $\mathcal{S}^{(o)}$ and $\mathcal{S}^{(f)}$, respectively; $\{\mathbf{s}^{(f)}_o, \tilde{\mathbf{s}}^{(f)}_o\}$ and $\{\mathbf{s}^{(f)}_f, \tilde{\mathbf{s}}^{(f)}_f\}$ are the corresponding MED constellation pairs for $\mathbf{p}^{(f)}$ using $\mathcal{S}^{(o)}$ and $\mathcal{S}^{(f)}$, respectively. We have the following result on the normalized MED difference.

Theorem 2: Letting $\mathcal{S}_d$ denote the set of $\{\mathbf{s}^{(o)}_o - \tilde{\mathbf{s}}^{(o)}_o, \mathbf{s}^{(o)}_f - \tilde{\mathbf{s}}^{(o)}_f, \mathbf{s}^{(f)}_o - \tilde{\mathbf{s}}^{(f)}_o, \mathbf{s}^{(f)}_f - \tilde{\mathbf{s}}^{(f)}_f\}$ and $\mathbf{A}^{(o)} = \sqrt{\text{diag}(\mathbf{p}^{(o)})}$, we have the following upper bound

$$\Delta\bar{d}^{\mathbf{p}}_{min} \triangleq \left|1 - \frac{d_{min}\left(\mathbf{H}, \mathbf{p}^{(f)}, \mathcal{S}^{(f)}\right)}{d_{min}\left(\mathbf{H}, \mathbf{p}^{(o)}, \mathcal{S}^{(o)}\right)}\right| \leq \left\|\mathbf{p}^{(o)} - \mathbf{p}^{(f)}\right\|_2 \cdot \max_{\mathbf{s}_d \in \mathcal{S}_d}\left\{\frac{\|\mathbf{H}\mathbf{s}_d\|^2_2}{\|\mathbf{H}\mathbf{A}^{(o)}\mathbf{s}_d\|^2_2}\right\}. \quad (17)$$

Generally, term $\max_{\mathbf{s}_d \in \mathcal{S}_d}\{\|\mathbf{H}\mathbf{s}_d\|^2_2/\|\mathbf{H}\mathbf{A}^{(o)}\mathbf{s}_d\|^2_2\}$ is finite, we have $\Delta\bar{d}^{\mathbf{p}}_{min} = O(\|\mathbf{p}^{(o)} - \mathbf{p}^{(f)}\|_2)$.

Proof: See Appendix B. ∎

Based on Theorem 2, the order of the asymptotic convergence rate of $\Delta\bar{d}^{\mathbf{p}}_{min}$ with respect to $\mathbf{p}^{(f)}$ is not larger than the order of $\|\mathbf{p}^{(o)} - \mathbf{p}^{(f)}\|_2$. This indicates that compared with the method using $\mathbf{p}^{(o)}$ to generate multi-dimensional constellations, the performance loss of using $\mathbf{p}^{(f)}$ can be sufficiently small if $\|\mathbf{p}^{(o)} - \mathbf{p}^{(f)}\|_2$ is sufficiently small. Hence, to avoid large performance loss of the system with fixed power allocation, we can set $\mathbf{p}^{(f)}$ close to $\mathbf{p}^{(o)}$. When the power vector is fixed, we can adopt $\mathcal{S}^{(f)}$ to generate the multi-dimensional constellation map.

We still qualitatively analyze the power allocation. Substituting $r = \beta r^{l_m}_{a,max}(z)$ and $r^l_{i,max}(z) = \sqrt{\frac{\lambda_i|l|}{\lambda_a|l_m|}}r^{l_m}_{a,max}(z)$ into Equation (2), the link gain can be rewritten as

$$g_i^l\left(\beta r_{a,max}^{l_m}(z), z\right) = \frac{\zeta_i^l \lambda_i^2}{(4\pi)^2 \left(d_{i,m}^l(z)\right)^2} \left(\frac{\lambda_a |l_m|}{\lambda_i |l|}\right)^{|l|} \beta^{2|l|} e^{|l|} e^{-\frac{\lambda_a |l_m|}{\lambda_i}\beta^2}. \quad (18)$$

Since $\beta_{i,max}^l = \sqrt{\frac{\lambda_i |l|}{\lambda_a |l_m|}}$ can represent the horizontal distance with the maximum link gain, we have that $g_i^l(\beta r_{a,max}^{l_m}(z), z)$ first increases as β increases within range $0 < \beta < \sqrt{\frac{\lambda_i |l|}{\lambda_a |l_m|}}$, and then decreases as β increases within range $\beta > \sqrt{\frac{\lambda_i |l|}{\lambda_a |l_m|}}$. Specially, for $l = 0$, $g_i^l(\beta r_{a,max}^{l_m}(z), z)$ always decreases as β increases. For any two OAM modes l_1 and l_2 satisfying $|l_1| > |l_2|$, $a_i^{l_1,l_2}(\beta, z)$ increases as β increases according to Equation (12). However, when both $|l_1|$ and $|l_2|$ are small and $|l_1|$ is close to $|l_2|$, there exist some positions where $a_i^{l_1,l_2}(\beta, z)$ is a moderate value (between 1 and 10). For short-range LOS links, $g_i^{l_1}(\beta r_{a,max}^{l_m}(z), z)$ is high within this range, and thus $g_i^{l_2}(\beta r_{a,max}^{l_m}(z), z)$ is also high due to moderate $a_i^{l_1,l_2}(\beta, z)$. We consider these regions as high-signal-strength regions, where the optimal power allocation is close to equal power allocation. Hence, the system can adopt the equal power allocation scheme as the fixed power allocation scheme, and generate the multi-dimensional constellation with a small performance loss.

In the regions where β is far away from $\beta_{i,max}^l$, $g_i^l(\beta r_{a,max}^{l_m}(z), z)$ is low, and the discrepancy between any two sub-channels is large. We consider these regions as the boundary regions (left or right region) of the OAM beam with mode l in the i-th sub-system. In these regions, the optimal power allocation scheme varies greatly, and the allocated power will be more likely to gather on sub-channels with high link gain. Hence, a fixed power allocation may lead to a larger performance loss.

IV. NUMERICAL RESULTS FOR MULTI-DIMENSIONAL CONSTELLATION MAP

In this section, numerical results are presented to verify the above theoretical analysis.

In the following, we consider the 60 GHz mmWave band, which has a 7 GHz unlicensed bandwidth and is widely used in short-range LOS environment [12]. We consider the OAM modes $\{0, +1, +2\}$, which are widely used in mmWave OAM system due to their simple implementation, especially for UCA antenna. We assume the noise power is $N_0 = 10^{-10}$, and the SNRs at the non-boundary positions are larger than 15dB, which is in line with the real short-range LOS scenario. Considering that the optimization dimension of the multi-dimensional constellation design is generally computationally intensive for our simulation, we set the number of sub-systems $I = 2$ and the number of multi-dimensional symbols $M = 32$ or 64.

We first consider the system with equal power allocation. Assume the frequency of the first sub-system is $f_1 = c/\lambda_1 = 60$ GHz, where c is the speed of light. The frequency interval is $\triangle f = 1$ GHz and $M = 64$. Consider

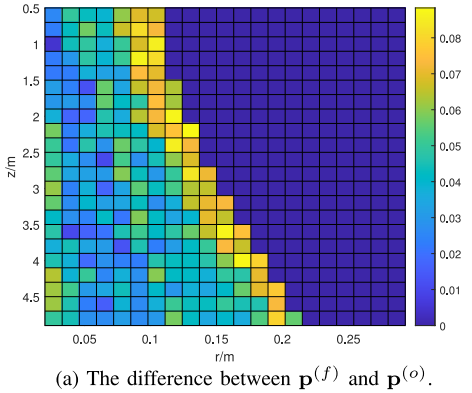

(a) The difference between $\mathbf{p}^{(f)}$ and $\mathbf{p}^{(o)}$.

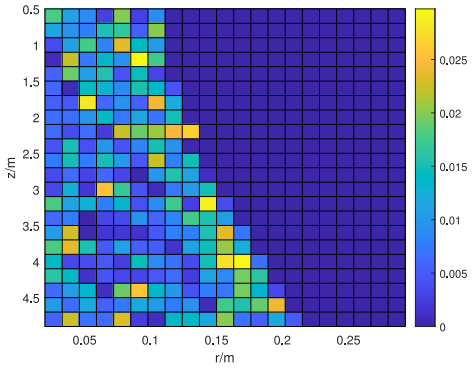

(b) The normalized MED difference $\Delta \bar{d}_{min}^{\mathbf{p}}$.

FIGURE 3. The performance loss of the system with equal power allocation and $\mathcal{L} = \{0, +1\}$.

the system with $\mathcal{L} = \{0, +1\}$. Figure 3a shows the power allocation difference $\|\mathbf{p}^{(o)} - \mathbf{p}^{(f)}\|_2$. It is seen that the difference is always small in the OAM beam region. The reason is that in the short-range LOS environment, the SNRs of all sub-channels are high, generally larger than 15dB when $N_0 = 10^{-10}$. Hence, the constellation symbols in $\mathcal{C}^{(o)}$ disperse more evenly on all sub-channels, and power vector $\mathbf{p}^{(o)}$ extracted from $\mathcal{C}^{(o)}$ is close to equal power allocation. Figure 3b shows the normalized MED difference $\Delta \bar{d}_{min}^{\mathbf{p}}$. We can observe that $\Delta \bar{d}_{min}^{\mathbf{p}}$ is always small, which is consistent with the feature in Theorem 2. Considering the system with $\mathcal{L} = \{0, +2\}$, we can see from Figure 4 that the power allocation difference and the normalized MED difference are also small in most positions. However, these differences will be very large in the boundary regions of the OAM beam with mode $+2$. The reason is that compared to the beam with mode $+1$, the beam with mode $+2$ has a larger divergence. In these boundary regions, the SNRs of the sub-channels with mode $+2$ are very low, and the constellation symbols in $\mathcal{C}^{(o)}$ will gather on the sub-channels with mode 0. Thus, if equal power allocation scheme is still adopted, the system will suffer a large performance loss.

According to the above results, the fixed power system in non-boundary region can adopt equal power allocation with a negligible performance loss. While in boundary region, equal power allocation among all sub-channels is not proper, and proper power pre-allocation scheme is required. Since the MED only depends on $\mathcal{S}^{(f)}$ at a certain position, we can

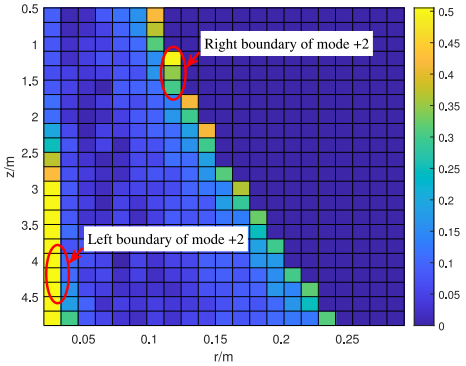

(a) The difference between $\mathbf{p}^{(f)}$ and $\mathbf{p}^{(o)}$.

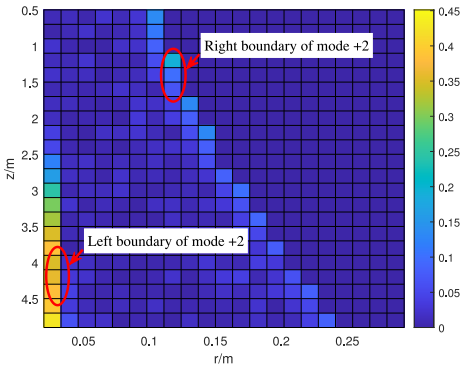

(b) The normalized MED difference $\Delta\bar{d}^{\mathbf{P}}_{min}$.

FIGURE 4. The performance loss of the system with equal power allocation and $\mathcal{L} = \{0, +2\}$.

adopt $\mathcal{S}^{(f)}$ rather than $\mathcal{C}^{(o)}$ to generate the multi-dimensional constellation map, which has the same features as that in the system with total power constraint.

Then, we focus on the system with total power constraint, and gives some examples to study the properties of multi-dimensional constellation maps. Figure 5 shows the multi-dimensional constellation maps with different system parameters. Different colors represent different categories, and it is observed that the OAM beam regions are classified into multiple categories. Each red curve in Figure 5 represents all the positions $(\beta r^{l_m}_{a,max}(z), z)$ with a fixed β, and it is seen that β can determine the horizontal distance from the beam axis ($r = 0$). We set $\lambda_a = \lambda_1$ and $l_m = +1$. It is seen that the region in each category diverge along the same direction as z increases, and in fact, this direction can be approximated as $r^{l_m}_{a,max}(z)$. According to the analysis above Theorem 1, the link gain ratio between any two sub-channels remains approximately unchanged for any positions $(\beta r^{l_m}_{a,max}(z), z)$ with fixed β, and thus the link gain matrices are nearly proportional, which further leads to a fixed constellation at these positions. Hence, Figure 5 verifies Theorem 1.

In Figure 5a, we consider the OAM mode set $\mathcal{L} = \{0, +1\}$, two carrier frequency $f_1 = 60$ GHz and $f_2 = 61$ GHz. When $l = +1$ and $i = 1$, $\beta^{+1}_{1,max} = \sqrt{\frac{\lambda_1|+1|}{\lambda_a|l_m|}} = 1$, and therefore the curve $\beta = 1$ represents the maximum link gain positions of the sub-channel with OAM mode $+1$ in the first sub-system.

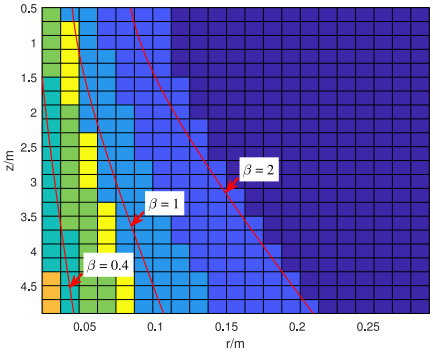

(a) $\mathcal{L} = \{0, +1\}$, $\triangle f = 1$ GHz, $M = 64$

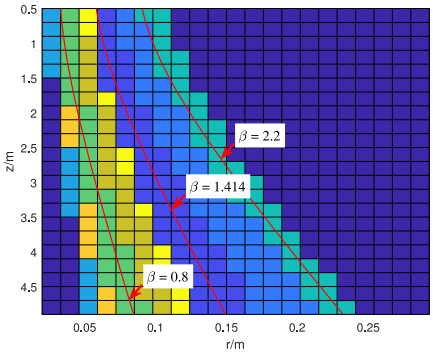

(b) $\mathcal{L} = \{0, +2\}$, $\triangle f = 1$ GHz, $M = 64$

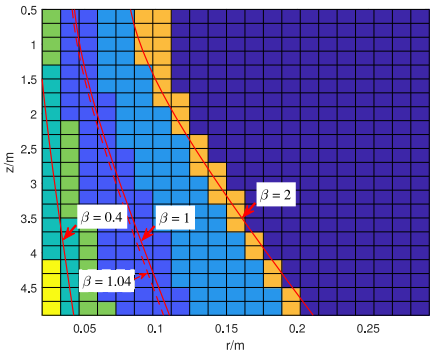

(c) $\mathcal{L} = \{0, +1\}$, $\triangle f = 5$ GHz, $M = 64$

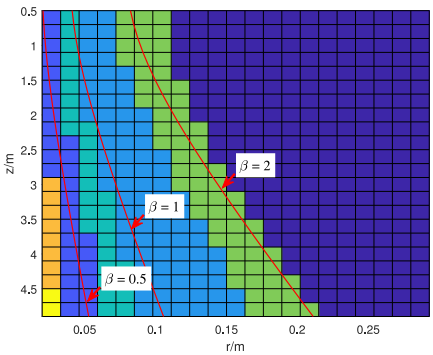

(d) $\mathcal{L} = \{0, +1\}$, $\triangle f = 1$ GHz, $M = 32$

FIGURE 5. Multi-dimensional constellation maps with $f_1 = 60$ GHz.

When $l = +1$ and $i = 2$, the maximum link gain positions almost overlap the curve $\beta = 1$ due to the small difference between f_1 and f_2. We also present the curves $\beta = 0.4$ and $\beta = 2$ in Figure 5a, which represent the positions of

the left and right boundary regions, respectively. The results shows that β can characterize the horizontal distance better than r. According to the analysis in Section III-C, it is easy to know that compared with the region $\beta < 1$, the channel matrix changes more slowly within $\beta > 1$. Hence, there are more categories in region $\beta < 1$ than those in region $\beta > 1$. Figures 5(b), 5(c) and 5(d) reveal similar features as those in Figure 5a. In Figure 5b, $\beta = 1.414$ represents the maximum link gain positions $\beta_{1,max}^{+2}$. Compared with Figure 5a, it is seen that the map in Figure 5b has more categories at the positions with small r. The reason is that the OAM beams with modes $+2$ have a larger beam divergence than the OAM beams with modes $+1$, so the channel condition changes rapidly in this region. Figure 5c shows the constellation map with two carrier frequency $f_1 = 60$ GHz and $f_2 = 65$ GHz, wherein $\beta = 1.04$ represents the maximum link gain positions $\beta_{2,max}^{+1}$. Compared with Figure 5a, the map in Figure 5c has slightly more categories. The reason is that when $\triangle f = 5$ GHz, the beam divergence of different carrier frequencies is slightly different, even if the OAM mode is the same. Figure 5d shows the constellation map with $M = 32$. It is seen that the region in each category diverges along the direction of a certain β, and the number of different categories in region $\beta > 1$ is larger than that in region $\beta < 1$. This confirms that the classification of a multi-dimensional constellation map mainly depends on positions rather than the modulation order.

Figures 6a and 6b show the normalized MED differences of the multi-dimensional constellation maps in Figure 5a and 5b, respectively. It is observed that the normalized MED differences are irregular in the whole OAM beam region. The reason is that the normalized MED differences are not uniformly continuous with respect to $\|\Delta\mathbf{H}\|_F$, which means that the normalized MED differences cannot be uniformly bounded even if the $\Delta\mathbf{H}$ are the same at different positions. Furthermore, the solution of the approximated optimization problem using iterative algorithm may be not global optimal. Hence, the normalized MED difference may fluctuate within the OAM beam region. This fluctuation can also be observed in Figures 3 and 4.

In summary, for short-range LOS links, multi-dimensional constellation map can be constructed as an offline look-up table to assign the constellation based on the position. Although there are multiple categories within the region with small r, the system can adopt a fixed multi-dimensional constellation at some positions with better channel condition. However, it is worth mentioning that as the number of OAM modes and wavelengths increases, the multi-dimensional constellation map will become more complicated. Hence, multi-dimensional constellation map can be adopted only when the number of sub-channels is small.

V. CONCLUSION

In this paper, we consider a mmWave WDM system with positioning information in short-range LOS environment. We also consider the OAM multiplexing in each wavelength

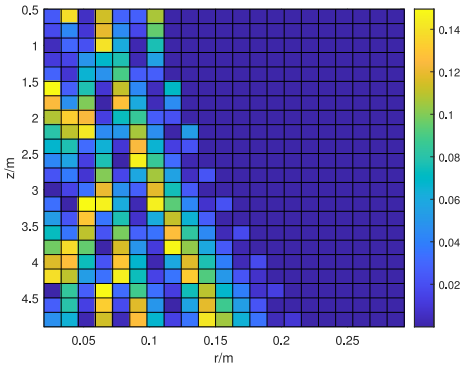

(a) $\mathcal{L} = \{0, +1\}$, $\triangle f = 1$ GHz

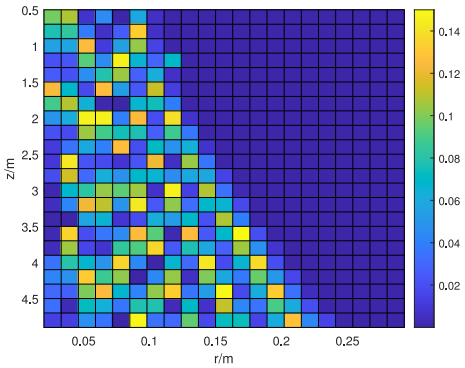

(b) $\mathcal{L} = \{0, +2\}$, $\triangle f = 1$ GHz

FIGURE 6. The normalized MED differences between using optimal constellation and mapped constellation.

part. Based on the quasi-static feature of the communication links, we have proposed a map-assisted approach to offline store the system parameters according to the transceiver's position and configure the system by employing these parameters when obtaining the position information. To reduce the storage and search complexity, we attempt to classify all considered positions into several categories and employ one fixed parameter in each category. We have applied the map-assisted method to the multi-dimensional constellation design problem. We have analyzed the features of OAM beams with different modes, and found that the link gain ratio between any two sub-channels remains unchanged at certain positions. Then, we have investigated the effect of channel condition on the multi-dimensional constellation design, and figured out that the normalized MED difference of fixed constellation is sufficiently small if link gain matrices are sufficiently close to be proportional. Moreover, we have also analyzed the effect of fixed-power allocation on the multi-dimensional constellation design, and found that the system adopting fixed-power allocation have a negligible performance loss if the difference between fixed-power vector and optimal power vector is small. Numerical results have verified the theoretical analysis.

APPENDIX A
PROOF OF THEOREM 1

According to the definition of MED, we have

$$
\begin{aligned}
&1-\frac{d_{min}\left(\mathbf{H}^{(2)},\mathcal{C}^{(1)}\right)}{d_{min}\left(\mathbf{H}^{(2)},\mathcal{C}^{(2)}\right)}\\
&=1-\frac{\|\mathbf{H}^{(2)}\left(\mathbf{x}^{(2)}_{\mathcal{C}^{(1)}}-\tilde{\mathbf{x}}^{(2)}_{\mathcal{C}^{(1)}}\right)\|_2}{\|\mathbf{H}^{(2)}\left(\mathbf{x}^{(2)}_{\mathcal{C}^{(2)}}-\tilde{\mathbf{x}}^{(2)}_{\mathcal{C}^{(2)}}\right)\|_2}\\
&=1-\frac{\|\left(\alpha\mathbf{H}^{(1)}+\Delta\mathbf{H}\right)\left(\mathbf{x}^{(2)}_{\mathcal{C}^{(1)}}-\tilde{\mathbf{x}}^{(2)}_{\mathcal{C}^{(1)}}\right)\|_2}{\|\mathbf{H}^{(2)}\left(\mathbf{x}^{(2)}_{\mathcal{C}^{(2)}}-\tilde{\mathbf{x}}^{(2)}_{\mathcal{C}^{(2)}}\right)\|_2}\\
&\overset{(a)}{\leq}1-\frac{\|\alpha\mathbf{H}^{(1)}\left(\mathbf{x}^{(2)}_{\mathcal{C}^{(1)}}-\tilde{\mathbf{x}}^{(2)}_{\mathcal{C}^{(1)}}\right)\|_2-\|\Delta\mathbf{H}\left(\mathbf{x}^{(2)}_{\mathcal{C}^{(1)}}-\tilde{\mathbf{x}}^{(2)}_{\mathcal{C}^{(1)}}\right)\|_2}{\|\mathbf{H}^{(2)}\left(\mathbf{x}^{(2)}_{\mathcal{C}^{(2)}}-\tilde{\mathbf{x}}^{(2)}_{\mathcal{C}^{(2)}}\right)\|_2}\\
&\overset{(b)}{\leq}1-\frac{\|\alpha\mathbf{H}^{(1)}\left(\mathbf{x}^{(1)}_{\mathcal{C}^{(1)}}-\tilde{\mathbf{x}}^{(1)}_{\mathcal{C}^{(1)}}\right)\|_2-\|\Delta\mathbf{H}\left(\mathbf{x}^{(2)}_{\mathcal{C}^{(1)}}-\tilde{\mathbf{x}}^{(2)}_{\mathcal{C}^{(1)}}\right)\|_2}{\|\mathbf{H}^{(2)}\left(\mathbf{x}^{(2)}_{\mathcal{C}^{(2)}}-\tilde{\mathbf{x}}^{(2)}_{\mathcal{C}^{(2)}}\right)\|_2}\\
&\overset{(c)}{\leq}1-\frac{\|\alpha\mathbf{H}^{(1)}\left(\mathbf{x}^{(1)}_{\mathcal{C}^{(2)}}-\tilde{\mathbf{x}}^{(1)}_{\mathcal{C}^{(2)}}\right)\|_2-\|\Delta\mathbf{H}\left(\mathbf{x}^{(2)}_{\mathcal{C}^{(1)}}-\tilde{\mathbf{x}}^{(2)}_{\mathcal{C}^{(1)}}\right)\|_2}{\|\mathbf{H}^{(2)}\left(\mathbf{x}^{(2)}_{\mathcal{C}^{(2)}}-\tilde{\mathbf{x}}^{(2)}_{\mathcal{C}^{(2)}}\right)\|_2}\\
&\overset{(d)}{\leq}1-\frac{\|\mathbf{H}^{(2)}\left(\mathbf{x}^{(1)}_{\mathcal{C}^{(2)}}-\tilde{\mathbf{x}}^{(1)}_{\mathcal{C}^{(2)}}\right)\|_2}{\|\mathbf{H}^{(2)}\left(\mathbf{x}^{(2)}_{\mathcal{C}^{(2)}}-\tilde{\mathbf{x}}^{(2)}_{\mathcal{C}^{(2)}}\right)\|_2}\\
&\quad+\frac{\|\Delta\mathbf{H}\left(\mathbf{x}^{(1)}_{\mathcal{C}^{(2)}}-\tilde{\mathbf{x}}^{(1)}_{\mathcal{C}^{(2)}}\right)\|_2+\|\Delta\mathbf{H}\left(\mathbf{x}^{(2)}_{\mathcal{C}^{(1)}}-\tilde{\mathbf{x}}^{(2)}_{\mathcal{C}^{(1)}}\right)\|_2}{\|\mathbf{H}^{(2)}\left(\mathbf{x}^{(2)}_{\mathcal{C}^{(2)}}-\tilde{\mathbf{x}}^{(2)}_{\mathcal{C}^{(2)}}\right)\|_2}\\
&\overset{(e)}{\leq}1-\frac{\|\mathbf{H}^{(2)}\left(\mathbf{x}^{(2)}_{\mathcal{C}^{(2)}}-\tilde{\mathbf{x}}^{(2)}_{\mathcal{C}^{(2)}}\right)\|_2}{\|\mathbf{H}^{(2)}\left(\mathbf{x}^{(2)}_{\mathcal{C}^{(2)}}-\tilde{\mathbf{x}}^{(2)}_{\mathcal{C}^{(2)}}\right)\|_2}\\
&\quad+\frac{\|\Delta\mathbf{H}\left(\mathbf{x}^{(1)}_{\mathcal{C}^{(2)}}-\tilde{\mathbf{x}}^{(1)}_{\mathcal{C}^{(2)}}\right)\|_2+\|\Delta\mathbf{H}\left(\mathbf{x}^{(2)}_{\mathcal{C}^{(1)}}-\tilde{\mathbf{x}}^{(2)}_{\mathcal{C}^{(1)}}\right)\|_2}{\|\mathbf{H}^{(2)}\left(\mathbf{x}^{(2)}_{\mathcal{C}^{(2)}}-\tilde{\mathbf{x}}^{(2)}_{\mathcal{C}^{(2)}}\right)\|_2}\\
&=\frac{\|\Delta\mathbf{H}\left(\mathbf{x}^{(1)}_{\mathcal{C}^{(2)}}-\tilde{\mathbf{x}}^{(1)}_{\mathcal{C}^{(2)}}\right)\|_2+\|\Delta\mathbf{H}\left(\mathbf{x}^{(2)}_{\mathcal{C}^{(1)}}-\tilde{\mathbf{x}}^{(2)}_{\mathcal{C}^{(1)}}\right)\|_2}{\|\mathbf{H}^{(2)}\left(\mathbf{x}^{(2)}_{\mathcal{C}^{(2)}}-\tilde{\mathbf{x}}^{(2)}_{\mathcal{C}^{(2)}}\right)\|_2}\\
&\overset{(f)}{\leq}\frac{\|\Delta\mathbf{H}\|_F\left(\|\mathbf{x}^{(1)}_{\mathcal{C}^{(2)}}-\tilde{\mathbf{x}}^{(1)}_{\mathcal{C}^{(2)}}\|_2+\|\mathbf{x}^{(2)}_{\mathcal{C}^{(1)}}-\tilde{\mathbf{x}}^{(2)}_{\mathcal{C}^{(1)}}\|_2\right)}{\|\mathbf{H}^{(2)}\left(\mathbf{x}^{(2)}_{\mathcal{C}^{(2)}}-\tilde{\mathbf{x}}^{(2)}_{\mathcal{C}^{(2)}}\right)\|_2}.
\end{aligned}
\tag{19}
$$

We give the detailed descriptions of the key steps as follows.

Step (a): It follows from the triangular inequality of norms.

Step (b): Since $\{\mathbf{x}^{(1)}_{\mathcal{C}^{(1)}},\tilde{\mathbf{x}}^{(1)}_{\mathcal{C}^{(1)}}\}$ is the MED constellation pair for $\alpha\mathbf{H}^{(1)}$ using $\mathcal{C}^{(1)}$, $\|\alpha\mathbf{H}^{(1)}(\mathbf{x}^{(1)}_{\mathcal{C}^{(1)}}-\tilde{\mathbf{x}}^{(1)}_{\mathcal{C}^{(1)}})\|_2\leq\|\alpha\mathbf{H}^{(1)}(\mathbf{x}^{(2)}_{\mathcal{C}^{(1)}}-\tilde{\mathbf{x}}^{(2)}_{\mathcal{C}^{(1)}})\|_2$ always holds, which leads to (b).

Step (c): According to the definition of MED, we have $d_{min}(\alpha\mathbf{H}^{(1)},\mathcal{C}^{(1)})=\|\alpha\mathbf{H}^{(1)}(\mathbf{x}^{(1)}_{\mathcal{C}^{(1)}}-\tilde{\mathbf{x}}^{(1)}_{\mathcal{C}^{(1)}})\|_2$ and $d_{min}(\alpha\mathbf{H}^{(1)},\mathcal{C}^{(2)})=\|\alpha\mathbf{H}^{(1)}(\mathbf{x}^{(1)}_{\mathcal{C}^{(2)}}-\tilde{\mathbf{x}}^{(1)}_{\mathcal{C}^{(2)}})\|_2$. Since $\mathcal{C}^{(1)}$ is the optimal constellation set of $\alpha\mathbf{H}^{(1)}$ and can lead to a maximum MED, we have $d_{min}(\alpha\mathbf{H}^{(1)},\mathcal{C}^{(1)})\geq d_{min}(\alpha\mathbf{H}^{(1)},\mathcal{C}^{(2)})$, which further leads to (c).

Step (d): It holds due to the reverse triangle inequality of norms.

Step (e): Similar to step (b), since $\{\mathbf{x}^{(2)}_{\mathcal{C}^{(2)}},\tilde{\mathbf{x}}^{(2)}_{\mathcal{C}^{(2)}}\}$ is the MED constellation pair for $\mathbf{H}^{(2)}$ using $\mathcal{C}^{(2)}$, $\|\mathbf{H}^{(2)}(\mathbf{x}^{(2)}_{\mathcal{C}^{(2)}}-\tilde{\mathbf{x}}^{(2)}_{\mathcal{C}^{(2)}})\|_2\leq\|\mathbf{H}^{(2)}(\mathbf{x}^{(1)}_{\mathcal{C}^{(2)}}-\tilde{\mathbf{x}}^{(1)}_{\mathcal{C}^{(2)}})\|_2$ always holds, which leads to (e).

Step (f): It holds due to the Cauchy-Schwarz inequality. Since $\mathbf{x}^{(2)}_{\mathcal{C}^{(2)}}$ and $\tilde{\mathbf{x}}^{(2)}_{\mathcal{C}^{(2)}}$ are two different constellations in $\mathcal{C}^{(2)}$, the term $\|\mathbf{H}^{(2)}(\mathbf{x}^{(2)}_{\mathcal{C}^{(2)}}-\tilde{\mathbf{x}}^{(2)}_{\mathcal{C}^{(2)}})\|_2$ is non-zero. Besides, the terms $\|\mathbf{x}^{(1)}_{\mathcal{C}^{(2)}}-\tilde{\mathbf{x}}^{(1)}_{\mathcal{C}^{(2)}}\|_2$ and $\|\mathbf{x}^{(2)}_{\mathcal{C}^{(1)}}-\tilde{\mathbf{x}}^{(2)}_{\mathcal{C}^{(1)}}\|_2$ are generally finite. Hence, term $(\|\mathbf{x}^{(1)}_{\mathcal{C}^{(2)}}-\tilde{\mathbf{x}}^{(1)}_{\mathcal{C}^{(2)}}\|_2+\|\mathbf{x}^{(2)}_{\mathcal{C}^{(1)}}-\tilde{\mathbf{x}}^{(2)}_{\mathcal{C}^{(1)}}\|_2)/\|\mathbf{H}^{(2)}(\mathbf{x}^{(2)}_{\mathcal{C}^{(2)}}-\tilde{\mathbf{x}}^{(2)}_{\mathcal{C}^{(2)}})\|_2$ is finite.

APPENDIX B
PROOF OF THEOREM 2

Note that $\mathcal{S}^{(o)}$ and $\mathcal{S}^{(f)}$ are the optimal constellations for $\mathbf{H}$ under $\mathbf{p}^{(o)}$ and $\mathbf{p}^{(f)}$, respectively. Then, we have

$$
\begin{aligned}
d_{min}\left(\mathbf{H},\mathbf{p}^{(f)},\mathcal{S}^{(f)}\right)&\geq d_{min}\left(\mathbf{H},\mathbf{p}^{(f)},\mathcal{S}^{(o)}\right)\\
d_{min}\left(\mathbf{H},\mathbf{p}^{(o)},\mathcal{S}^{(o)}\right)&\geq d_{min}\left(\mathbf{H},\mathbf{p}^{(o)},\mathcal{S}^{(f)}\right).
\end{aligned}
\tag{20}
$$

Hence, the following inequalities always hold

$$
\begin{aligned}
1-\frac{d_{min}\left(\mathbf{H},\mathbf{p}^{(f)},\mathcal{S}^{(f)}\right)}{d_{min}\left(\mathbf{H},\mathbf{p}^{(o)},\mathcal{S}^{(o)}\right)}&\geq 1-\frac{d_{min}\left(\mathbf{H},\mathbf{p}^{(f)},\mathcal{S}^{(f)}\right)}{d_{min}\left(\mathbf{H},\mathbf{p}^{(o)},\mathcal{S}^{(f)}\right)}\\
1-\frac{d_{min}\left(\mathbf{H},\mathbf{p}^{(f)},\mathcal{S}^{(f)}\right)}{d_{min}\left(\mathbf{H},\mathbf{p}^{(o)},\mathcal{S}^{(o)}\right)}&\leq 1-\frac{d_{min}\left(\mathbf{H},\mathbf{p}^{(f)},\mathcal{S}^{(o)}\right)}{d_{min}\left(\mathbf{H},\mathbf{p}^{(o)},\mathcal{S}^{(o)}\right)}.
\end{aligned}
\tag{21}
$$

Based on Equation (21), the normalized MED difference satisfies

$$
\begin{aligned}
&\left|1-\frac{d_{min}\left(\mathbf{H},\mathbf{p}^{(f)},\mathcal{S}^{(f)}\right)}{d_{min}\left(\mathbf{H},\mathbf{p}^{(o)},\mathcal{S}^{(o)}\right)}\right|\\
&\leq\max\left\{\left|1-\frac{d_{min}\left(\mathbf{H},\mathbf{p}^{(f)},\mathcal{S}^{(f)}\right)}{d_{min}\left(\mathbf{H},\mathbf{p}^{(o)},\mathcal{S}^{(f)}\right)}\right|,\left|1-\frac{d_{min}\left(\mathbf{H},\mathbf{p}^{(f)},\mathcal{S}^{(o)}\right)}{d_{min}\left(\mathbf{H},\mathbf{p}^{(o)},\mathcal{S}^{(o)}\right)}\right|\right\}.
\end{aligned}
\tag{22}
$$

Letting $\mathbf{A}^{(o)}=\sqrt{\text{diag}(\mathbf{p}^{(o)})}$ and $\mathbf{A}^{(f)}=\sqrt{\text{diag}(\mathbf{p}^{(f)})}$, we first consider the following normalized MED difference,

$$
\begin{aligned}
&\left|1-\frac{d_{min}\left(\mathbf{H},\mathbf{p}^{(f)},\mathcal{S}^{(f)}\right)}{d_{min}\left(\mathbf{H},\mathbf{p}^{(o)},\mathcal{S}^{(f)}\right)}\right|\\
&\overset{(a)}{\leq}\left|1-\frac{d^2_{min}\left(\mathbf{H},\mathbf{p}^{(f)},\mathcal{S}^{(f)}\right)}{d^2_{min}\left(\mathbf{H},\mathbf{p}^{(o)},\mathcal{S}^{(f)}\right)}\right|\\
&=\left|1-\frac{\|\mathbf{H}\mathbf{A}^{(f)}\left(\mathbf{s}^{(f)}_f-\tilde{\mathbf{s}}^{(f)}_f\right)\|^2_2}{\|\mathbf{H}\mathbf{A}^{(o)}\left(\mathbf{s}^{(o)}_f-\tilde{\mathbf{s}}^{(o)}_f\right)\|^2_2}\right|\\
&\overset{(b)}{\leq}\max\left\{\left|1-\frac{\|\mathbf{H}\mathbf{A}^{(f)}\left(\mathbf{s}^{(f)}_f-\tilde{\mathbf{s}}^{(f)}_f\right)\|^2_2}{\|\mathbf{H}\mathbf{A}^{(o)}\left(\mathbf{s}^{(f)}_f-\tilde{\mathbf{s}}^{(f)}_f\right)\|^2_2}\right|,\right.\\
&\qquad\left.\left|1-\frac{\|\mathbf{H}\mathbf{A}^{(f)}\left(\mathbf{s}^{(o)}_f-\tilde{\mathbf{s}}^{(o)}_f\right)\|^2_2}{\|\mathbf{H}\mathbf{A}^{(o)}\left(\mathbf{s}^{(o)}_f-\tilde{\mathbf{s}}^{(o)}_f\right)\|^2_2}\right|\right\}.
\end{aligned}
\tag{23}
$$

Step (a) follows from the relation $|1-x|\leq|1-x|\cdot|1+x|$, where $x\geq 0$. Step (b) holds due to the following statement. Since $\{\mathbf{s}^{(f)}_f,\tilde{\mathbf{s}}^{(f)}_f\}$ is the MED constellation pair for $\mathbf{p}^{(f)}$ using

$\mathcal{S}^{(f)}$, $\|\mathbf{H}\mathbf{A}^{(f)}(\mathbf{s}_f^{(f)}-\tilde{\mathbf{s}}_f^{(f)})\|_2^2 \le \|\mathbf{H}\mathbf{A}^{(f)}(\mathbf{s}_f^{(o)}-\tilde{\mathbf{s}}_f^{(o)})\|_2^2$ always holds. Similarly, since $\{\mathbf{s}_f^{(o)},\tilde{\mathbf{s}}_f^{(o)}\}$ is the MED constellation pair for $\mathbf{p}^{(o)}$ using $\mathcal{S}^{(f)}$, $\|\mathbf{H}\mathbf{A}^{(o)}(\mathbf{s}_f^{(o)}-\tilde{\mathbf{s}}_f^{(o)})\|_2^2 \le \|\mathbf{H}\mathbf{A}^{(o)}(\mathbf{s}_f^{(f)}-\tilde{\mathbf{s}}_f^{(f)})\|_2^2$ always holds. Hence, we have

$$1-\frac{\|\mathbf{H}\mathbf{A}^{(f)}\left(\mathbf{s}_f^{(f)}-\tilde{\mathbf{s}}_f^{(f)}\right)\|_2^2}{\|\mathbf{H}\mathbf{A}^{(o)}\left(\mathbf{s}_f^{(o)}-\tilde{\mathbf{s}}_f^{(o)}\right)\|_2^2} \le 1-\frac{\|\mathbf{H}\mathbf{A}^{(f)}\left(\mathbf{s}_f^{(f)}-\tilde{\mathbf{s}}_f^{(f)}\right)\|_2^2}{\|\mathbf{H}\mathbf{A}^{(o)}\left(\mathbf{s}_f^{(o)}-\tilde{\mathbf{s}}_f^{(o)}\right)\|_2^2}$$
$$1-\frac{\|\mathbf{H}\mathbf{A}^{(f)}\left(\mathbf{s}_f^{(f)}-\tilde{\mathbf{s}}_f^{(f)}\right)\|_2^2}{\|\mathbf{H}\mathbf{A}^{(o)}\left(\mathbf{s}_f^{(o)}-\tilde{\mathbf{s}}_f^{(o)}\right)\|_2^2} \ge 1-\frac{\|\mathbf{H}\mathbf{A}^{(f)}\left(\mathbf{s}_f^{(o)}-\tilde{\mathbf{s}}_f^{(o)}\right)\|_2^2}{\|\mathbf{H}\mathbf{A}^{(o)}\left(\mathbf{s}_f^{(o)}-\tilde{\mathbf{s}}_f^{(o)}\right)\|_2^2}, \tag{24}$$

which leads to (b). Then, it follows

$$\begin{aligned}
&\left|1-\frac{\|\mathbf{H}\mathbf{A}^{(f)}\left(\mathbf{s}_f^{(f)}-\tilde{\mathbf{s}}_f^{(f)}\right)\|_2^2}{\|\mathbf{H}\mathbf{A}^{(o)}\left(\mathbf{s}_f^{(f)}-\tilde{\mathbf{s}}_f^{(f)}\right)\|_2^2}\right| \\
&= \frac{\left|\sum_{i=1}^N \frac{|h_i|^2}{N_i}\left(p_i^{(o)}-p_i^{(f)}\right)|\mathbf{s}_f^{(f)}(i)-\tilde{\mathbf{s}}_f^{(f)}(i)|^2\right|}{\|\mathbf{H}\mathbf{A}^{(o)}\left(\mathbf{s}_f^{(f)}-\tilde{\mathbf{s}}_f^{(f)}\right)\|_2^2} \\
&\overset{(c)}{\le} \frac{\sum_{i=1}^N \frac{|h_i|^2}{N_i}|p_i^{(o)}-p_i^{(f)}|\cdot|\mathbf{s}_f^{(f)}(i)-\tilde{\mathbf{s}}_f^{(f)}(i)|^2}{\|\mathbf{H}\mathbf{A}^{(o)}\left(\mathbf{s}_f^{(f)}-\tilde{\mathbf{s}}_f^{(f)}\right)\|_2^2} \\
&\overset{(d)}{\le} \frac{\left(\sum_{i=1}^N \frac{|h_i|^4}{N_i^2}|\mathbf{s}_f^{(f)}(i)-\tilde{\mathbf{s}}_f^{(f)}(i)|^4\right)^{\frac{1}{2}}\cdot\left(\sum_{i=1}^N|p_i^{(o)}-p_i^{(f)}|^2\right)^{\frac{1}{2}}}{\|\mathbf{H}\mathbf{A}^{(o)}\left(\mathbf{s}_f^{(f)}-\tilde{\mathbf{s}}_f^{(f)}\right)\|_2^2} \\
&\overset{(e)}{\le} \frac{\left(\sum_{i=1}^N \frac{|h_i|^2}{N_i}|\mathbf{s}_f^{(f)}(i)-\tilde{\mathbf{s}}_f^{(f)}(i)|^2\right)\cdot\left\|\mathbf{p}^{(o)}-\mathbf{p}^{(f)}\right\|_2}{\|\mathbf{H}\mathbf{A}^{(o)}\left(\mathbf{s}_f^{(f)}-\tilde{\mathbf{s}}_f^{(f)}\right)\|_2^2} \\
&= \frac{\|\mathbf{H}\left(\mathbf{s}_f^{(f)}-\tilde{\mathbf{s}}_f^{(f)}\right)\|_2^2\cdot\left\|\mathbf{p}^{(o)}-\mathbf{p}^{(f)}\right\|_2}{\|\mathbf{H}\mathbf{A}^{(o)}\left(\mathbf{s}_f^{(f)}-\tilde{\mathbf{s}}_f^{(f)}\right)\|_2^2}.
\end{aligned} \tag{25}$$

Step (c) follows from the inequality of $|\sum_k v_k| \le \sum_k |v_k|$. Step (d) holds due to the Cauchy-Schwarz inequality. Step (e) holds due to the inequality of $\sum_k v_k^2 \le (\sum_k v_k)^2$ with $v_k \ge 0$. Similarly, we can obtain the upper bound of $|1-\|\mathbf{H}\mathbf{A}^{(f)}(\mathbf{s}_f^{(o)}-\tilde{\mathbf{s}}_f^{(o)})\|_2^2/\|\mathbf{H}\mathbf{A}^{(o)}(\mathbf{s}_f^{(o)}-\tilde{\mathbf{s}}_f^{(o)})\|_2^2|$.

Hence, the upper bound of Equation (23) can be further rewritten as

$$\left|1-\frac{d_{min}\left(\mathbf{H},\mathbf{p}^{(f)},\mathcal{S}^{(f)}\right)}{d_{min}\left(\mathbf{H},\mathbf{p}^{(o)},\mathcal{S}^{(f)}\right)}\right| \le \left\|\mathbf{p}^{(o)}-\mathbf{p}^{(f)}\right\|_2 \cdot \max\left\{\frac{\|\mathbf{H}\left(\mathbf{s}_f^{(f)}-\tilde{\mathbf{s}}_f^{(f)}\right)\|_2^2}{\|\mathbf{H}\mathbf{A}^{(o)}\left(\mathbf{s}_f^{(f)}-\tilde{\mathbf{s}}_f^{(f)}\right)\|_2^2}, \frac{\|\mathbf{H}\left(\mathbf{s}_f^{(o)}-\tilde{\mathbf{s}}_f^{(o)}\right)\|_2^2}{\|\mathbf{H}\mathbf{A}^{(o)}\left(\mathbf{s}_f^{(o)}-\tilde{\mathbf{s}}_f^{(o)}\right)\|_2^2}\right\}. \tag{26}$$

Using similar steps in Equations (23)-(26), we obtain

$$\left|1-\frac{d_{min}\left(\mathbf{H},\mathbf{p}^{(f)},\mathcal{S}^{(o)}\right)}{d_{min}\left(\mathbf{H},\mathbf{p}^{(o)},\mathcal{S}^{(o)}\right)}\right| \le \left\|\mathbf{p}^{(o)}-\mathbf{p}^{(f)}\right\|_2 \cdot \max\left\{\frac{\|\mathbf{H}\left(\mathbf{s}_o^{(o)}-\tilde{\mathbf{s}}_o^{(o)}\right)\|_2^2}{\|\mathbf{H}\mathbf{A}^{(o)}\left(\mathbf{s}_o^{(o)}-\tilde{\mathbf{s}}_o^{(o)}\right)\|_2^2}, \frac{\|\mathbf{H}\left(\mathbf{s}_o^{(f)}-\tilde{\mathbf{s}}_o^{(f)}\right)\|_2^2}{\|\mathbf{H}\mathbf{A}^{(o)}\left(\mathbf{s}_o^{(f)}-\tilde{\mathbf{s}}_o^{(f)}\right)\|_2^2}\right\}. \tag{27}$$

Substituting Equations (26) and (27) into Equation (22), it yields

$$\begin{aligned}
&\left|1-\frac{d_{min}\left(\mathbf{H},\mathbf{p}^{(f)},\mathcal{S}^{(f)}\right)}{d_{min}\left(\mathbf{H},\mathbf{p}^{(o)},\mathcal{S}^{(o)}\right)}\right| \\
&\le \left\|\mathbf{p}^{(o)}-\mathbf{p}^{(f)}\right\|_2 \cdot \max_{\mathbf{s}_d\in\mathcal{S}_d}\left\{\frac{\|\mathbf{H}\mathbf{s}_d\|_2^2}{\|\mathbf{H}\mathbf{A}^{(o)}\mathbf{s}_d\|_2^2}\right\},
\end{aligned} \tag{28}$$

where $\mathcal{S}_d$ is the set of $\{\mathbf{s}_o^{(o)}-\tilde{\mathbf{s}}_o^{(o)}, \mathbf{s}_o^{(f)}-\tilde{\mathbf{s}}_o^{(f)}, \mathbf{s}_f^{(o)}-\tilde{\mathbf{s}}_f^{(o)}, \mathbf{s}_f^{(f)}-\tilde{\mathbf{s}}_f^{(f)}\}$. Generally, the constellation points of $\mathcal{S}^{(f)}$ do not only distribute on the sub-channels with zero power, when $\mathbf{p}^{(f)}$ is set reasonably. Hence, the term $\|\mathbf{H}\mathbf{A}^{(o)}\mathbf{s}_d\|_2^2$ is non-zero and the term $\max_{\mathbf{s}_d\in\mathcal{S}_d}\{\|\mathbf{H}\mathbf{s}_d\|_2^2/\|\mathbf{H}\mathbf{A}^{(o)}\mathbf{s}_d\|_2^2\}$ is finite.

ACKNOWLEDGMENT

The authors would like to thank Dr. Qian Gao (Futurewei Technology) for his constructive comments and suggestions that improve the quality of this paper.

REFERENCES

[1] Q. Qi, X. Chen, C. Zhong, and Z. Zhang, "Integrated sensing, computation and communication in B5G cellular Internet of Things," *IEEE Trans. Wireless Commun.*, vol. 20, no. 1, pp. 332–344, Jan. 2021.

[2] H.-J. Song and T. Nagatsuma, "Present and future of terahertz communications," *IEEE Trans. THz Sci. Technol.*, vol. 1, no. 1, pp. 256–263, Sep. 2011.

[3] S. Sun et al., "Investigation of prediction accuracy, sensitivity, and parameter stability of large-scale propagation path loss models for 5G wireless communications," *IEEE Trans. Veh. Technol.*, vol. 65, no. 5, pp. 2843–2860, May 2016.

[4] M. Mezzavilla et al., "End-to-end simulation of 5G mmWave networks," *IEEE Commun. Surveys Tuts.*, vol. 20, no. 3, pp. 2237–2263, 3rd Quart., 2018.

[5] X. Ge, R. Zi, X. Xiong, Q. Li, and L. Wang, "Millimeter wave communications with OAM-SM scheme for future mobile networks," *IEEE J. Sel. Areas Commun.*, vol. 35, no. 9, pp. 2163–2177, Sep. 2017.

[6] Y. Yan et al., "High-capacity millimetre-wave communications with orbital angular momentum multiplexing," *Nat. Commun.*, vol. 5, p. 4876, Mar. 2014.

[7] Y. Ren et al., "Line-of-sight millimeter-wave communications using orbital angular momentum multiplexing combined with conventional spatial multiplexing," *IEEE Trans. Wireless Commun.*, vol. 16, no. 5, pp. 3151–3161, May 2017.

[8] X. Hui et al., "Multiplexed millimeter wave communication with dual orbital angular momentum (OAM) mode antennas," *Sci. Rep.*, vol. 5, May 2015, Art. no. 10148.

[9] Y. Yan et al., "32-Gbit/s 60-GHz millimeter-wave wireless communication using orbital angular momentum and polarization multiplexing," in *Proc. IEEE Int. Conf. Commun. (ICC)*, 2016, pp. 1–6.

[10] H. Sasaki et al., "Experiment on over-100-Gbps wireless transmission with OAM-MIMO multiplexing system in 28-GHz band," in *Proc. IEEE Global Commun. Conf. (GLOBECOM)*, 2018, pp. 1–6.

[11] W. Zhang, S. Zheng, Y. Chen, X. Jin, H. Chi, and X. Zhang, "Orbital angular momentum-based communications with partial arc sampling receiving," *IEEE Commun. Lett.*, vol. 20, no. 7, pp. 1381–1384, Jul. 2016.
[12] P. Liu, M. Di Renzo, and A. Springer, "Line-of-sight spatial modulation for indoor mmWave communication at 60 GHz," *IEEE Trans. Wireless Commun.*, vol. 15, no. 11, pp. 7373–7389, Nov. 2016.
[13] P. Liu, J. Blumenstein, N. S. Perović, M. Di Renzo, and A. Springer, "Performance of generalized spatial modulation MIMO over measured 60GHz indoor channels," *IEEE Trans. Commun.*, vol. 66, no. 1, pp. 133–148, Jan. 2018.
[14] X. Gao, L. Dai, S. Han, C.-L. I, and R. W. Heath, "Energy-efficient hybrid analog and digital precoding for mmWave MIMO systems with large antenna arrays," *IEEE J. Sel. Areas Commun.*, vol. 34, no. 4, pp. 998–1009, Apr. 2016.
[15] X. Gao, L. Dai, S. Han, C.-L. I, and X. Wang, "Reliable beamspace channel estimation for millimeter-wave massive MIMO systems with lens antenna array," *IEEE Trans. Wireless Commun.*, vol. 16, no. 9, pp. 6010–6021, Sep. 2017.
[16] S. A. Busari, K. M. S. Huq, S. Mumtaz, L. Dai, and J. Rodriguez, "Millimeter-wave massive MIMO communication for future wireless systems: A survey," *IEEE Commun. Surveys Tuts.*, vol. 20, no. 2, pp. 836–869, 2nd Quart., 2018.
[17] M. Kokshoorn, H. Chen, Y. Li, and B. Vucetic, "Beam-on-graph: Simultaneous channel estimation for mmWave MIMO systems with multiple users," *IEEE Trans. Commun.*, vol. 66, no. 7, pp. 2931–2946, Jul. 2018.
[18] R. Zhang, Y. Zhang, Z. Zhong, and S. X. Lu, "The correlation properties of subchannel fading for non-continuous carrier aggregation based on indoor ultra-wideband measurement," in *Proc. IEEE Global Commun. Conf. (GLOBECOM)*, 2012, pp. 4071–4077.
[19] B. Liu, C. Gong, J. Cheng, and Z. Xu, "Power allocation over broad spectra optical wireless scattering communication based on link gain correlation," *IEEE Trans. Commun.*, vol. 67, no. 10, pp. 6980–6993, Oct. 2019.
[20] C.-X. Wang, J. Bian, J. Sun, W. Zhang, and M. Zhang, "A survey of 5G channel measurements and models," *IEEE Commun. Surveys Tuts.*, vol. 20, no. 4, pp. 3142–3168, 4th Quart., 2018.
[21] A. Maltsev, R. Maslennikov, A. Sevastyanov, A. Khoryaev, and A. Lomayev, "Experimental investigations of 60 GHz WLAN systems in office environment," *IEEE J. Sel. Areas Commun.*, vol. 27, no. 8, pp. 1488–1499, Oct. 2009.
[22] R. Chen, W.-X. Long, X. Wang, and L. Jiandong, "Multi-mode OAM radio waves: Generation, angle of arrival estimation and reception with UCAs," *IEEE Trans. Wireless Commun.*, vol. 19, no. 10, pp. 6932–6947, Oct. 2020.
[23] R. Chen, H. Xu, M. Moretti, and J. Li, "Beam steering for the misalignment in UCA-based OAM communication systems," *IEEE Wireless Commun. Lett.*, vol. 7, no. 4, pp. 582–585, Aug. 2018.
[24] G. Zheng, C. Gong, and Z. Xu, "Constrained partial group decoding with max–min fairness for multi-color multi-user visible light communication," *IEEE Trans. Commun.*, vol. 67, no. 12, pp. 8573–8584, Dec. 2019.
[25] S. Zheng, X. Hui, X. Jin, H. Chi, and X. Zhang, "Transmission characteristics of a twisted radio wave based on circular travelling-wave antenna," *IEEE Trans. Antennas Propag.*, vol. 63, no. 4, pp. 1530–1536, Apr. 2015.
[26] W. Zhang et al., "Mode division multiplexing communication using microwave orbital angular momentum: An experimental study," *IEEE Trans. Wireless Commun.*, vol. 16, no. 2, pp. 1308–1318, Feb. 2017.
[27] E. Basar, "Orbital angular momentum with index modulation," *IEEE Trans. Wireless Commun.*, vol. 17, no. 3, pp. 2029–2037, Mar. 2018.
[28] J. Luo, L. Fan, and H. Li, "Indoor positioning systems based on visible light communication: State of the art," *IEEE Commun. Surveys Tuts.*, vol. 19, no. 4, pp. 2871–2893, 4th Quart., 2017.
[29] C. Cai, Y. Zhao, J. Zhang, L. Wang, and J. Wang, "Experimental demonstration of an underwater wireless optical link employing orbital angular momentum (OAM) modes with fast auto-alignment system," in *Proc. Opt. Fiber Commun. Conf. Exhibit. (OFC)*, 2019, pp. 1–3.
[30] F. Liu, M. Chen, W. Jiang, X. Jin, and Z. Xu, "Effective auto-alignment and tracking of transceivers for visible-light communication in data centres," in *Proc. Broadband Access Commun. Technol. XIII*, 2019, Art. no. 109450N.
[31] J. Xu, "Generation of Laguerre–Gaussian modes by aperture or array sources," *IEEE Trans. Antennas Propag.*, vol. 67, no. 1, pp. 415–429, Jan. 2019.
[32] L. Allen, M. W. Beijersbergen, R. J. C. Spreeuw, and J. P. Woerdman, "Orbital angular momentum of light and the transformation of Laguerre–Gaussian laser modes," *Phys. Rev. A*, vol. 45, no. 11, pp. 8185–8189, Jun. 1992.
[33] M. Oldoni et al., "Space-division demultiplexing in orbital-angular-momentum-based MIMO radio systems," *IEEE Trans. Antennas Propag.*, vol. 63, no. 10, pp. 4582–4587, Oct. 2015.
[34] Q. Gao, R. Wang, Z. Xu, and Y. Hua, "DC-informative joint color-frequency modulation for visible light communications," *J. Lightw. Technol.*, vol. 33, no. 11, pp. 2181–2188, Jun. 1, 2015.
[35] J. V. Servera et al., "Gradient-based automatic lookup table generator for radiative transfer models," *IEEE Trans. Geosci. Remote Sens.*, vol. 57, no. 2, pp. 1040–1048, Feb. 2019.

YUAN WANG received the B.S. degree from the Dalian University of Technology, Dalian, China, in 2017. He is currently pursuing the Ph.D. degree with the University of Science and Technology of China, Hefei, China.

CHEN GONG (Senior Member, IEEE) received the B.S. degree in electrical engineering and mathematics (minor) from Shanghai Jiaotong University, Shanghai, China, in 2005, the M.S. degree in electrical engineering from Tsinghua University, Beijing, China, in 2008, and the Ph.D. degree from Columbia University, New York City, NY, USA, in 2012. He was a Senior Systems Engineer with Qualcomm Research, San Diego, CA, USA, from 2012 to 2013. He is currently a Faculty Member with the University of Science and Technology of China. His research interests in wireless communications, optical wireless communications, and signal processing. He was selected by the Young 1000 Talent Program of China Government in 2014 and awarded by the Hong Kong Qiushi Outstanding Young Researcher Award in 2016.

NUO HUANG received the B.S. degree in electronics and information engineering from the Huazhong University of Science and Technology, Wuhan, China, in 2012, and the Ph.D. degree in information and communication engineering from the National Mobile Communications Research Laboratory, Southeast University, Nanjing, China, in 2019. He is currently a Research Associate with the Department of Electronic Engineering and Information Science, University of Science and Technology of China. From December 2015 to June 2017, he was a visiting student with the Department of Electrical Engineering, Columbia University, New York, NY, USA. His research interests include resource allocation and transceiver design in wireless (optical) communications. He was selected by the National Postdoctoral Program for Innovative Talents in 2019.

ZHENGYUAN XU (Senior Member, IEEE) received the B.S. and M.S. degrees from Tsinghua University, China, and the Ph.D. degree from the Stevens Institute of Technology, USA. He was a Tenured Full Professor with the University of California at Riverside and later with Tsinghua University, before he joined the University of Science and Technology of China. He was the Founding Director of the multi-campus Center for Ubiquitous Communication by Light, University of California, and the Founding Director of Wireless-Optical Communications Key Laboratory, Chinese Academy of Sciences. He was a Distinguished Expert and the Chief Scientist of the National Key Basic Research Program of China. He has published over 400 international journal and conference papers, and coauthored a book titled *Visible Light Communications: Modulation and Signal Processing* which has been selected by IEEE Series on Digital and Mobile Communication and published by Wiley-IEEE Press. His research focuses on Petahertz communications, optical wireless communications, mobile networking, artificial intelligence, wireless big data, sensing, ranging, and localization. He has been on the Elsevier annual list of Most Cited Chinese Researchers since 2014. He has served as an Associate Editor for different IEEE/OSA journals and was a Founding Co-Chair of IEEE Workshop on Optical Wireless Communications in 2010.